

REPORT DOCUMENTATION PAGE			Form Approved OMB No. 0704-0188	
<small>Public reporting burden for this collection of information is estimated to average 1 hour per response, including the time for reviewing instructions, searching existing data sources, gathering and maintaining the data needed, and completing and reviewing the collection of information. Send comments regarding this burden estimate or any other aspect of this collection of information, including suggestions for reducing this burden, to Washington Headquarters Services, Directorate for Information Operations and Reports, 1215 Jefferson Davis Highway, Suite 1204, Arlington, VA 22202-4302, and to the Office of Management and Budget, Paperwork Reduction Project (0704-0188), Washington, DC 20503.</small>				
1. AGENCY USE ONLY (Leave blank)	2. REPORT DATE 5.Sep.02	3. REPORT TYPE AND DATES COVERED THESIS		
4. TITLE AND SUBTITLE AZURE DYES AS REDOX MEDIATORS FOR ELECTROCHEMICAL BIOSENSING		5. FUNDING NUMBERS		
6. AUTHOR(S) CAPT LIM LUCY				
7. PERFORMING ORGANIZATION NAME(S) AND ADDRESS(ES) UNIVERSITY OF TEXAS SAN ANTONIO		8. PERFORMING ORGANIZATION REPORT NUMBER  CI02-521		
9. SPONSORING/MONITORING AGENCY NAME(S) AND ADDRESS(ES) THE DEPARTMENT OF THE AIR FORCE AFIT/CIA, BLDG 125 2950 P STREET WPAFB OH 45433		10. SPONSORING/MONITORING AGENCY REPORT NUMBER		
11. SUPPLEMENTARY NOTES				
12a. DISTRIBUTION AVAILABILITY STATEMENT Unlimited distribution In Accordance With AFI 35-205/AFIT Sup 1		12b. DISTRIBUTION CODE  DISTRIBUTION STATEMENT A: Approved for Public Release - Distribution Unlimited		
13. ABSTRACT (Maximum 200 words)				
<div style="font-size: 2em; font-weight: bold; margin: 0;">20021029 025</div>				
14. SUBJECT TERMS			15. NUMBER OF PAGES 74	
			16. PRICE CODE	
17. SECURITY CLASSIFICATION OF REPORT	18. SECURITY CLASSIFICATION OF THIS PAGE	19. SECURITY CLASSIFICATION OF ABSTRACT	20. LIMITATION OF ABSTRACT	

This is a copy of an original placed in the  
bound thesis.

*Forster*

AZURE DYES AS REDOX MEDIATORS FOR  
ELECTROCHEMICAL BIOSENSING

APPROVED BY SUPERVISING COMMITTEE:

*W. Gorski*

Dr. Waldemar Gorski, Chair

*Stephen B. Bach*

Dr. Stephen B. H. Bach

*George Negrete*

Dr. George Negrete

*Petr Hochmann*

Dr. Petr Hochmann

DISTRIBUTION STATEMENT A:  
Approved for Public Release -  
Distribution Unlimited

Accepted:

*Dorothy H. H. H.*

Dean of Graduate Studies

# AZURE DYES AS REDOX MEDIATORS FOR ELECTROCHEMICAL BIOSENSING

Lucy Lim, M.S.  
The University of Texas at San Antonio, 2002

Supervising Professor: Dr. Waldemar Gorski

The research presented in this thesis was composed of three parts. In the first part, the kinetics of the redox mediation between the azure dyes and the enzyme glucose oxidase was investigated. Electrochemical studies showed that azure dyes were fast mediators when dissolved in aqueous solutions. In the second part, the covalent immobilization of azure dyes in the biopolymeric matrix of chitosan was explored in order to design a reagentless glucose biosensor. These investigations indicated that the length of the tethering molecule was a crucial parameter, which controlled the mediation efficiency in the biosensor. The third part of this work was devoted to the preparation and characterization of a carbon paste-based electrochemical biosensor for glucose. The paste was modified with an azure eosinate mediator and glucose oxidase, and its analytical performance was tested under the conditions of diffusional and convective mass transport.

## TABLE OF CONTENTS

Acknowledgements .....	iii
------------------------	-----

Abstract .....	iv
----------------	----

### PART 1

1.0 Coupling of the Glucose Oxidase/Glucose System to an Electrode. Redox Mediation with Azure Dyes .....	1
1.0.1 Introduction .....	1
1.1 Experimental .....	7
1.1.1 Chemicals .....	7
1.1.2 Separation Techniques .....	8
1.1.3 Electrochemical Instrumentation and Data Collection .....	10
1.2 Theoretical .....	11
1.2.1 Electrochemical Setup and Techniques .....	11
1.3 Results and Discussion .....	21
1.3.1 Azure Dyes as Homogeneous Oxidants for Glucose Oxidase .....	21
1.4 Conclusions – Part 1 .....	29

### PART 2

2.0 Immobilization of Azure Dyes and Glucose Oxidase on the Electrode Surface: A Reagentless Glucose Biosensor Design .....	30
2.0.1 Introduction .....	30

2.1	Immobilization of Azure Dyes Within the Chitosan Matrix .....	31
2.2	Results and Discussion .....	39
2.2.1	Electrochemical Testing of the Chitosan-Tether-Azure-GOx Films .....	39
2.3	Conclusions – Part 2 .....	49

### PART 3

3.0	Paste Enzyme Electrode Based on Azure Eosinate Artificial Mediator .....	50
3.0.1	Introduction .....	50
3.1	Results and Discussion .....	52
3.1.1	Azure Eosinate Dyes as Homogeneous Oxidants for Glucose Oxidase .....	52
3.1.2	Paste Azure Eosinate A Glucose Oxidase Electrodes as Biosensors for Glucose .....	56
3.2	Conclusions – Part 3 .....	66
	References .....	71

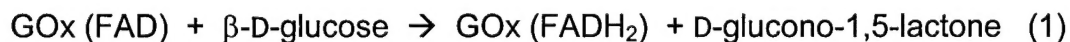
Vita

## PART 1

### 1.0 Coupling of the Glucose Oxidase/Glucose System to an Electrode. Redox Mediation with Azure Dyes

#### 1.0.1 Introduction

Electrochemical biosensors based on enzymes are appealing because they integrate the selectivity of an enzymatic reaction with the high sensitivity of electrochemical signal transduction. The most frequently used enzymes in electrochemical biosensors belong to a class called oxidoreductases.<sup>1</sup> Oxidoreductases catalyze the redox transformations of their substrates. The enzyme glucose oxidase (GOx) is the most stable oxidoreductase. It catalyzes the oxidation of glucose, which is its substrate, to gluconolactone, according to the following sequence of reactions<sup>2</sup>:



where FAD and FADH<sub>2</sub> are the oxidized and reduced forms, respectively, of flavin adenine dinucleotide, the catalytically active site of GOx. The mechanistic details of the FAD/FADH<sub>2</sub> system are presented in Figure 1.

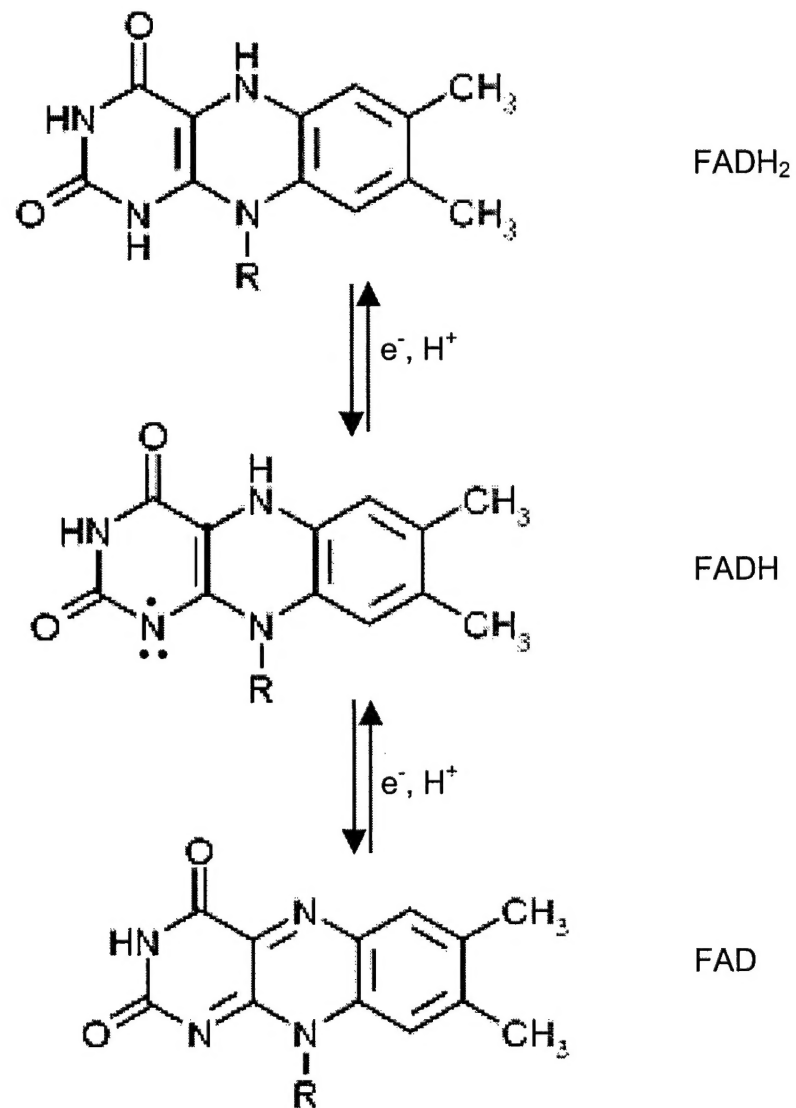


**Figure 1.** The oxidation of the FADH<sub>2</sub> center of glucose oxidase.

The enzymatic oxidation of glucose has been used as a model system in the development of electrochemical biosensors because GOx is a highly active enzyme that is readily available in high purity, and is relatively inexpensive. In addition, the stability and activity of the enzyme is sustained through several pH and temperature ranges, and through repetitive experimentations.

When coupled to an electrode, the enzymatic reaction can be transduced into an electrochemical signal (current) based on any one of the following processes:

- a) monitoring either the formation of  $\text{H}_2\text{O}_2$  or the consumption of  $\text{O}_2$  in reaction (2).<sup>3-7</sup>
- b) reoxidation of the enzyme with artificial redox mediators that replace  $\text{O}_2$  in reaction (2).<sup>8-25</sup>
- c) direct reoxidation of a reduced form of the enzyme at the electrode surface.<sup>26-29</sup>

The direct reoxidation process (c) is the most compelling because of its simplicity. However, this approach to biosensor design is difficult to realize because the redox active FAD is buried deep within the enzyme (Figure 2). The distance between the FAD and the surface of the enzyme is ca. 13-18 Å.<sup>30</sup> Consequently, the distance between the FAD and the electrode surface is too long to permit an effective electron transfer between them.<sup>31</sup> On the other hand, the oxygen based signal transduction (a) is less attractive because it requires the presence of oxygen in the samples and fluctuations in oxygen concentrations can lead to false positive or negative signals.

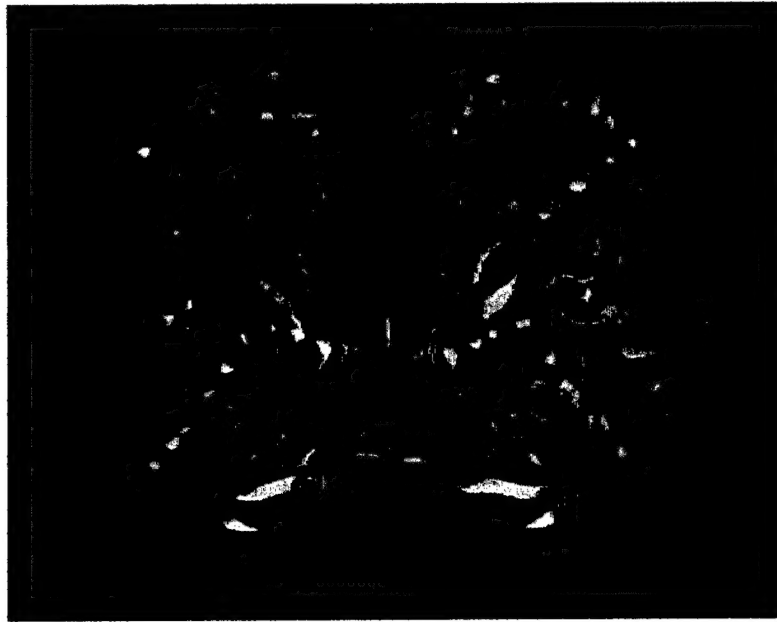


**Figure 2.** Ribbon structure of the glucose oxidase enzyme. The FAD active site lies within the funnel shaped cavity of the molecule. ([www-biol.paisley.ac.uk](http://www-biol.paisley.ac.uk))

The approach (b), which is based on artificial mediators, is probably the most favorable because it can eliminate the pitfalls associated with fluctuating oxygen levels in samples, particularly those of biological origin.

The artificial mediators have to fulfill some basic requirements in order to support the high sensitivity and stability of a biosensor. They must have:

- (a) fast kinetics of electron exchange with the enzyme
- (b) fast kinetics of electron exchange with the electrode surface
- (c) a low standard potential
- (d) good stability in both oxidized and reduced forms
- (e) functional groups to permit their immobilization on an electrode surface

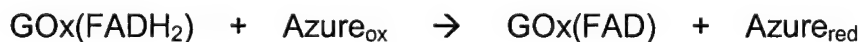
Several artificial mediators for coupling the enzymatic reactions to electrodes have been explored. Among the earliest were ferrocene derivatives, which have been used in disposable glucose sensors sold commercially for diabetics.<sup>11,12</sup> A list of other redox mediators included: osmium bipyridine complexes<sup>13,14</sup>, substituted bipyridine complexes of iron, ruthenium and osmium<sup>15</sup>, cyano- and amino-complexes of ruthenium<sup>16,17</sup>, octacyanotungstate(IV) and octacyanomolybdate(IV)<sup>18</sup>, ferricyanide,<sup>19</sup> viologens,<sup>20</sup> quinones,<sup>21</sup> tetrathiafulvalene,<sup>22</sup> diaminodurene,<sup>23</sup> C<sub>60</sub>,<sup>24</sup> and violuric acid.<sup>25</sup> However, most of these mediators have high standard potentials, which translates into high operating potentials for biosensors. Consequently, such biosensors are prone to interferences from redox active species, such as ascorbic acid, uric acid, acetaminophen, which are present in physiological samples. In such a

case, selective electrode coatings have to be designed to alleviate the problems of such interferences.

This thesis is devoted to the systematic examination of azure dyes as redox mediators for amperometric glucose biosensors, based on glucose oxidase. These dyes fulfill most of the requirements for an efficient mediation of enzymatic reactions. For example, our work showed that they react fast with the enzyme and carbon electrodes. In addition, they have low standard potentials, good stability, and amino groups that can be used for their immobilization in amperometric biosensors.

In view of these advantageous properties of azure dyes, it is surprising that only a handful of papers on their biosensor applications have been reported. The azure dyes have been used to mediate redox of dihydronicotinamide adenine dinucleotide<sup>32</sup>, cholesterol oxidase<sup>33</sup>, and nitrate reductase.<sup>34</sup> However, these reports have not involved concepts that are explored in this thesis.

The first part of my thesis concentrates on the kinetics of the reaction between selected azure dyes (A, B, and C) and the reduced form of glucose oxidase:



## 1.1 EXPERIMENTAL

### 1.1.1 Chemicals.

Glucose oxidase (GOx) from *Aspergillus niger* (EC 1.1.3.4, type X-S, 208.8 units  $\text{mg}^{-1}$ ), chitosan (poly (D-glucosamine); MW  $1.9 - 3.1 \times 10^5$ ; 75-85 % deacetylation),  $\alpha$ -D-glucose, L-ascorbic acid, uric acid, 4-acetamidophenol, Azure dyes A, B, C and Azure A and B Eosinate, glutaric dialdehyde (GDI) 50 % w/v, 1,6-hexamethylene diisocyanate (HDI), polyethylene glycol (PEG), neutral alumina oxide, graphite carbon with a particle size of 1-2  $\mu\text{m}$ , mineral oil, methanol, acetonitrile, acryloyl chloride, benzene, chloroform, hydrochloric acid and potassium nitrate were all purchased from Sigma-Aldrich. Poly (ethylene glycol) (n) diglycidyl ether (PEGDGE) was purchased from Polysciences. The metallographic polishing cloth (Mark V Lab) and polishing alumina with particle sizes of 0.3 and 0.05  $\mu\text{m}$  were purchased from Buehler. The 3M™ sand paper was purchased from Wal-Mart. Sodium hydroxide, sodium phosphate monobasic and dibasic were purchased from EM Science.

Phosphate buffer, 0.05 M, was prepared using both monobasic and dibasic sodium phosphate dissolved in deionized water. The pH was adjusted to  $7.40 \pm 0.05$  by adding saturated NaOH solution and using a Corning 340 pH meter. All solutions were prepared using water purified by a Barnstead NANOpure cartridge system ( $\geq 18 \text{ M}\Omega \text{ cm}$ ). Ultrahigh purity argon was used to deoxygenate solutions, if needed.

A 0.3 wt. % chitosan stock solution was prepared by dissolving chitosan flakes in heated 0.05 M HCl. The solution was cooled to room temperature and filtered using a 0.45  $\mu\text{m}$  Millex-HA syringe filter unit (Millipore). Aliquots of the chitosan stock solution were diluted to 0.1 wt. % with deionized water and the pH adjusted to  $5.4 \pm 0.3$  with aqueous NaOH. Fresh chitosan solutions were prepared every 4 weeks. Solid  $\alpha$ -D-glucose was dissolved in buffer to prepare a 1.0 M glucose stock solution. Fresh glucose stock solutions were prepared every 4 weeks. The solution was allowed to stand overnight for mutarotation before storage at 4°C.

### 1.1.2 Separation Techniques

In the synthesis of a modified chitosan, three separation techniques (dialysis, extraction, and column chromatography) were used to remove unreacted species from a reaction mixture. The dialysis cell (ScienceWare™) is shown in Figure 3. The cell is composed of two chambers, which are separated by the size-exclusion membrane. The membrane with a molecular cut-off of 500 Da was used to separate low molecular weight unreacted species from chitosan ( $\sim 10^5$  Da). In theory, such a membrane is permeable to species with a molecular weight below 500 Da. The dialysis experiments were performed in a continuous mode. Deionized water was slowly ( $\sim 0.1 \text{ mL min}^{-1}$ ) pumped through the dialysate chamber, while the other chamber contained a reaction mixture. The dialysis experiments lasted from 1 to 3 days.

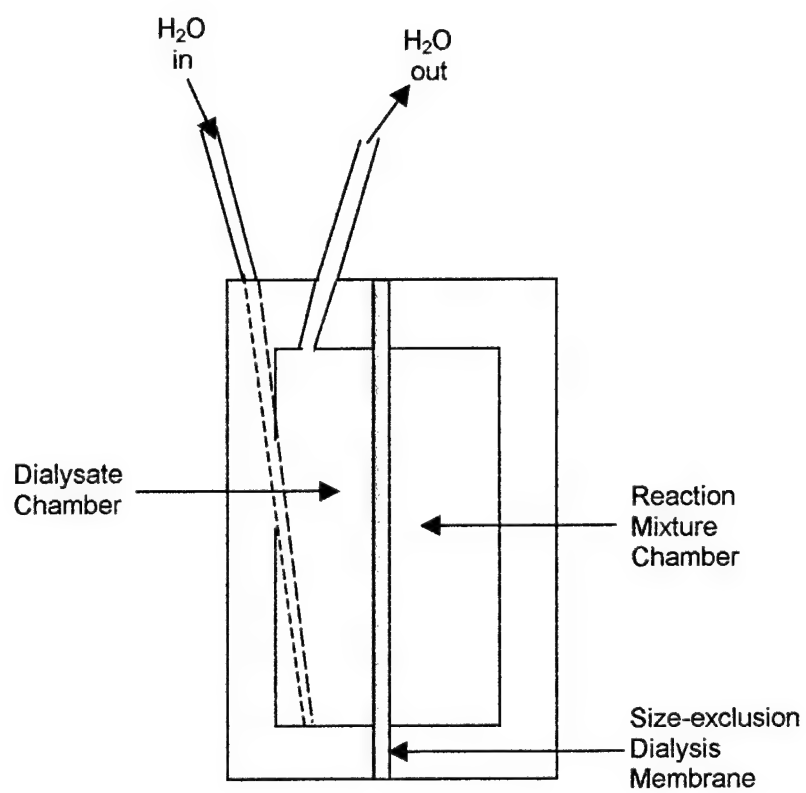


**Figure 3:** Schematic diagram of a dialysis cell.

Separation by extraction was performed in a separation funnel using chloroform or benzene as extracting solvents. In the chromatographic separations, a column packed with neutral alumina oxide was used. The reaction mixture was placed on top of the column and eluted slowly with methanol – ethylacetate (1:3) solvent.

### **1.1.3 Electrochemical Instrumentation and Data Collection.**

Electrochemical experiments were performed using a CH Instruments, Model 832, electrochemical detector. A conventional three-electrode system was used, employing a 3-mm diameter glassy carbon electrode (Bioanalytical Systems, Inc.) as the working electrode, a platinum wire as the auxiliary electrode, and a Ag/AgCl/3MNaCl as the reference electrode. All experiments were performed at room temperature ( $21 \pm 1^\circ\text{C}$ ).

Ultraviolet/visible spectroscopic (UV/vis) measurements were performed using a Hewlett Packard 8453 UV/vis diode array spectrophotometer and 1 cm quartz cuvettes. The cuvettes were cleaned with methanol and deionized water.

The glassy carbon electrodes were first wet-polished on 3M™ fine sandpaper (grain 2000). They were then polished to mirror smoothness on metallographic Alpha A polishing cloth (Mark V Lab), using successively smaller alumina particles (0.3 and 0.05  $\mu\text{m}$  diameter) suspended in deionized water. Following each polishing step, the residual slurry remaining on the electrode was removed by a 20 s ultrasonication in deionized water. All experiments were repeated at least three times and the means of measurements are presented with the standard deviations.

The glassy carbon electrodes were modified with chitosan film using the casting technique. In a typical procedure, 20  $\mu\text{L}$  of the casting solution was placed on the electrode surface and allowed to evaporate for 1 hr at room temperature. The casting solutions were prepared by mixing the chemically modified chitosan with an enzyme solution in a ceramic well of a ceramic plate.

Carbon pastes were prepared by mixing graphite powder, azure eosinate, glucose oxidase and oil. The dry components were thoroughly ground for 30 min before the oil was added to make a paste with dough-like consistency. Two paste compositions were used, each containing either 28 or 40 wt. % azure eosinate. The glucose oxidase percentage was kept constant at 25 wt. %, while the amount of graphite carbon was varied. The paste was pressed manually into the electrode cavity (3 mm diameter, 2 mm depth) and then smoothed on weigh paper until a flat surface was obtained and excess paste was removed. The prepared electrodes were stored in air at room temperature when not in use.

## **1.2 THEORETICAL**

### **1.2.1 Electrochemical Setup and Techniques.**

Figure 4 shows the electrochemical cell that was used in all the electrochemical experiments. The cell is composed of three electrodes, which are immersed in a solution containing a background electrolyte and redox active species under study (analyte). The electrochemical process of interest takes place at the working

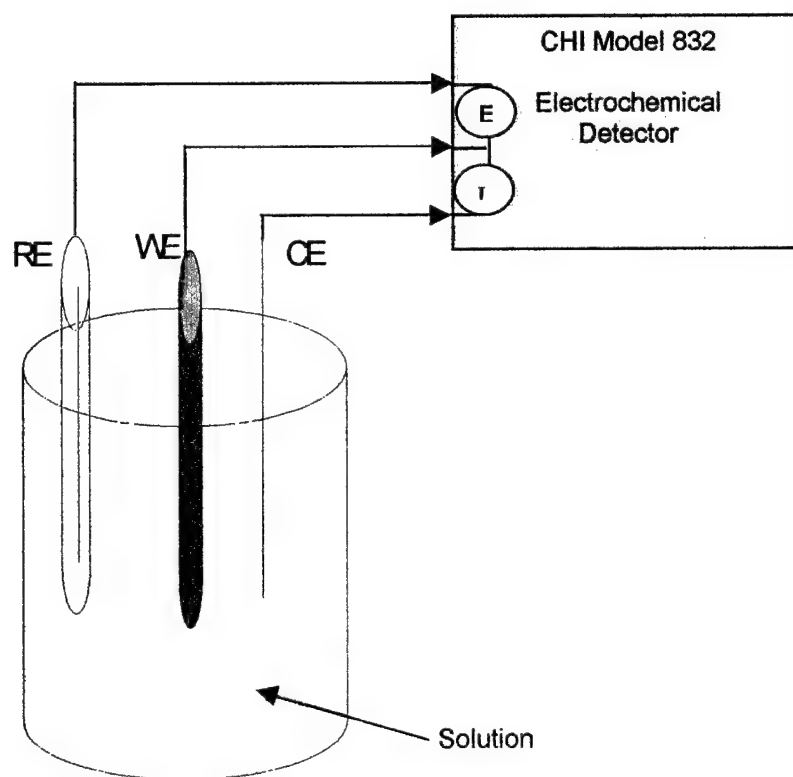


**Figure 4.** Three electrode cell used in electrochemical measurements. WE – working electrode, RE – reference electrode, CE – counter electrode. A potential  $E$  is measured between WE and RE, and current  $I$  is measured between WE and CE.

electrode. The potential applied to the working electrode is measured versus the reference electrode. The reference electrode is composed of Ag/AgCl/3MNaCl, which has a potential equal to +197 mV vs. Standard Hydrogen Electrode. The current flowing through the working electrode is measured with the help of the counter electrode. The role of the counter electrode is to minimize the potential drop  $IR$  ( $I$  – current,  $R$  – resistance of solution between the working and reference electrodes). In addition, the counter electrode protects the reference electrode by passing the majority of current flowing in the electrolytic cell. The solutions for electrochemical experiments have to contain a background electrolyte in order to minimize the migration of analyte ions. Background electrolytes are made of strong electrolytes, e.g. salts, strong acids or bases, which supply ions that take over the migrational transport in the solution.

Two electrochemical techniques that were used are cyclic voltammetry and chronoamperometry.<sup>35</sup> In cyclic voltammetry, a ramp of a potential  $E$  (Figure 5) is applied to the working electrode and the resulting current  $I$  flowing through it is measured. The plot of  $E$  vs.  $I$  is called a cyclic voltammogram. Figure 6 displays a typical cyclic voltammogram for a reversible electrode process occurring at the working electrode. It is assumed that only the reduced form Red is present initially in the solution. Therefore, a positive-going potential ramp is chosen for the forward scan. The  $E_{\text{initial}}$  is selected to be far from the characteristic standard potential  $E^\circ$  for the Ox/Red redox couple. As the applied potential approaches  $E^\circ$ , an oxidation (anodic) current begins to increase until a peak is reached. After traversing the scanning potential at least  $90/n$  mV beyond the peak, the direction of the potential ramp is

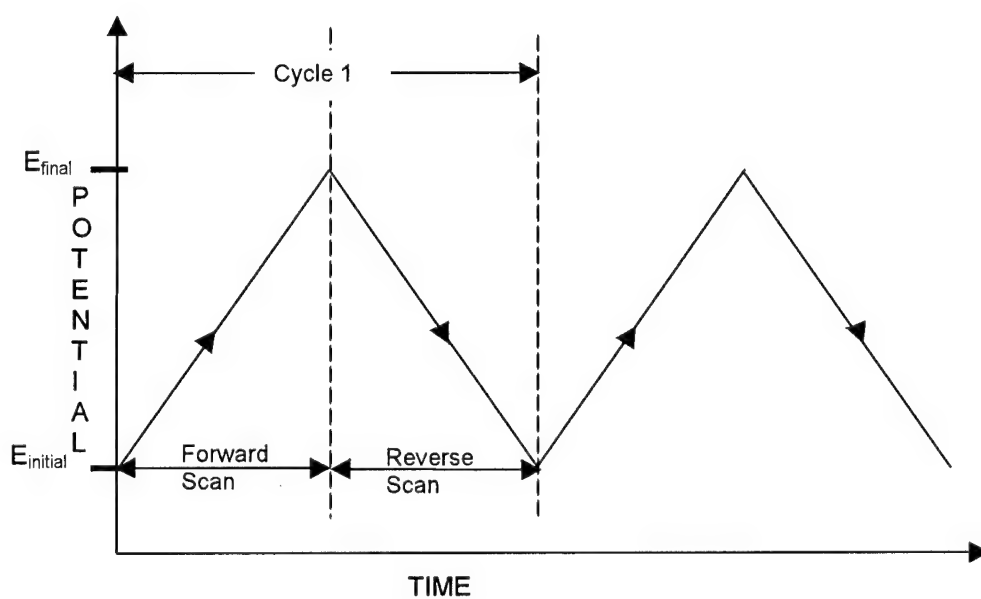


**Figure 5.** Potential – time function applied to the working electrode in cyclic voltammetry.

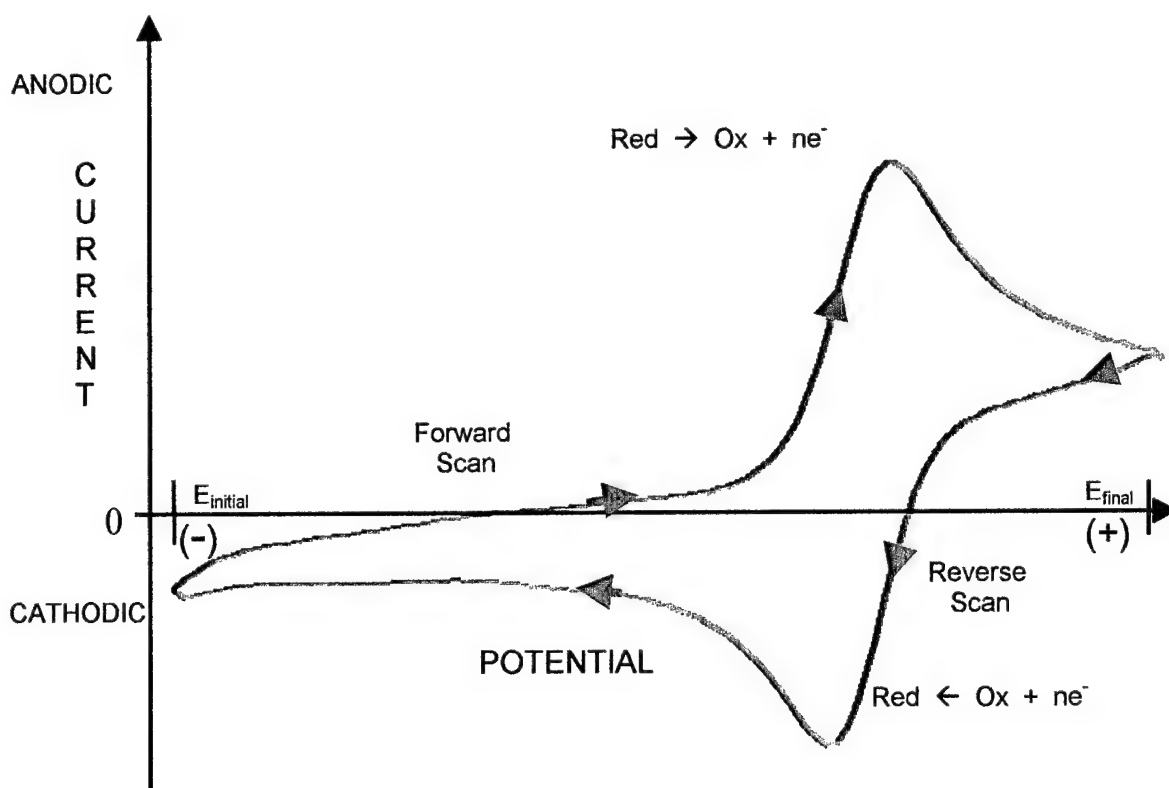


**Figure 6.** Typical cyclic voltammogram for a reversible  $\text{Red} \leftrightarrow \text{Ox} + n\text{e}^-$  electrode process recorded at a working electrode in a quiescent solution.

reversed at  $E_{\text{final}}$ . During the reverse scan, Ox species, which were generated in the forward scan and accumulated near the electrode surface, are re-reduced back to Red resulting in a cathodic peak.

The characteristic peaks in the cyclic voltammogram originate from the diffusion layer that develops at the electrode surface. For example, a decrease of the concentration of Red in the diffusion layer (due to the  $\text{Red} \rightarrow \text{Ox} + n\text{e}^-$  reaction), coupled with an expansion of the diffusion layer thickness in time, is responsible for the formation of an anodic peak on cyclic voltammograms. In other words, the current peaks observed in cyclic voltammograms reflect the development of changing concentrations gradients near the electrode surface.

The peak current,  $I_d$ , for the electrode process controlled by diffusion is described by the Randles-Sevcik equation<sup>35</sup>

$$I_d = 0.4463nFAC (nF/RT)^{1/2} \nu^{1/2} D_{\text{med}}^{1/2} \quad (3)$$

where  $I_d$  is the diffusion controlled peak current in Amperes,  $n$  is the number of transferred electrons,  $A$  is the area of the working electrode ( $\text{cm}^2$ ),  $C$  is the concentration of the analyte ( $\text{mol mL}^{-1}$ ),  $F$  is the Faraday constant,  $T$  is the temperature (K),  $\nu$  is the scan rate ( $\text{V s}^{-1}$ ), and  $D_{\text{med}}$  is the diffusion coefficient of a mediator (analyte) ( $\text{cm}^2 \text{sec}^{-1}$ ).

In the second technique used in this work, a constant potential is applied to the working electrode and the current is measured as a function of time. The potential is

selected from the potential range beyond the voltametric peak. At such a potential, the electrode reaction is forced to proceed at maximum rate, which is limited only by mass transfer in the solution. The chronoamperometric technique was used in conjunction with convective mass transfer of solution species to the working electrode. In the first approach, called a batch experiment, the solution was stirred and small volumes of a stock solution of analyte were added. After each addition of the analyte, the current should increase because it is directly proportional to the concentration of analyte. In addition, the current should stay constant after each analyte addition because a convective transport due to the stirring continuously supplies analyte species to the electrode surface. As a result, a chronoamperogram recorded in the batch experiment is typically composed of a series of current steps (Figure 7).

In the second approach, chronoamperometry was used in conjunction with a flow system. In such a system, a carrier solution flows toward the working electrode, which is positioned at the solution outlet. Two configurations of the flow system were used. In the first one (Figure 8A), called a flow injection analysis (FIA), the analyte solution is injected into the carrier solution using an injection valve. When the bolus of the analyte solution from the sample loop reaches the electrode, the current increases (Figure 8B) because of the redox process that takes place at the electrode. After a short time, the current decreases back to the background level because the analyte species becomes diluted at the electrode surface by the carrier solution. The resultant current peak is proportional to the concentration of analyte.

In the second configuration of a flow system, two reservoirs are used (Figure 9A). One reservoir contains a carrier solution, and the other is filled with a carrier

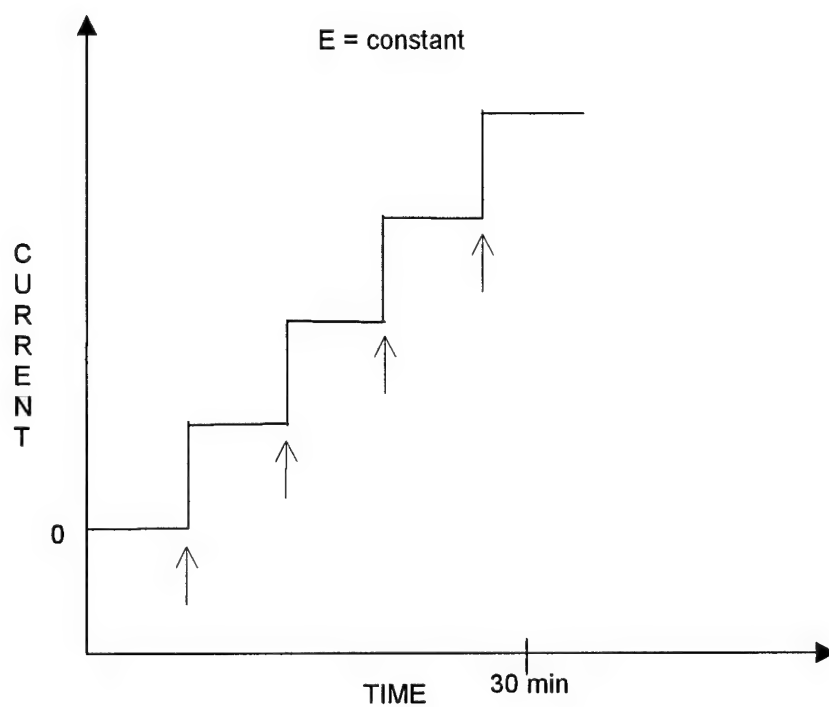


**Figure 7.** A schematic drawing of a chronoamperogram obtained with convective mass transport in a batch experiment. Arrows indicate successive additions of analyte to a stirred solution.

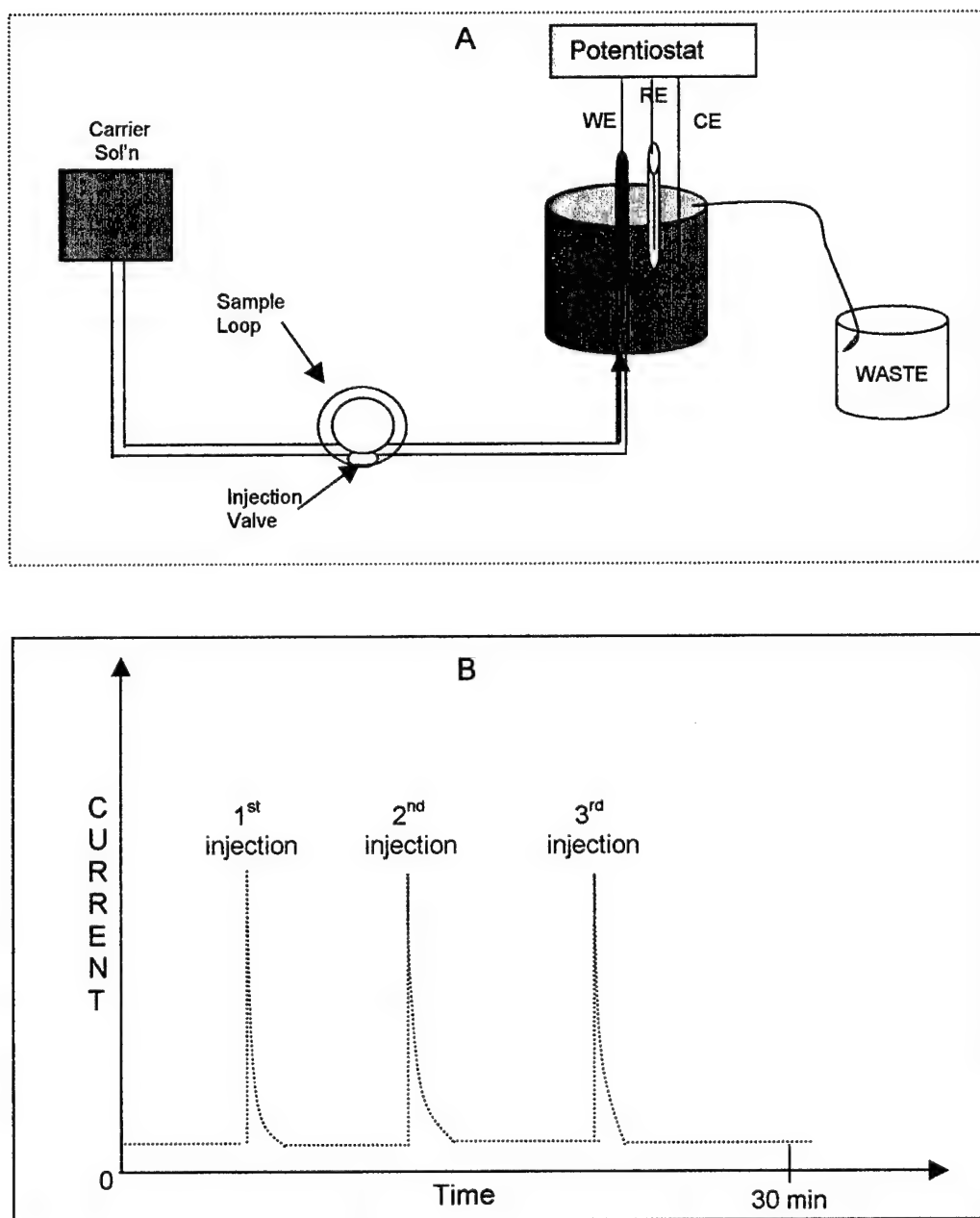


**Figure 8.** (A) Flow injection analysis system (FIA) used to test biosensors; (B) A schematic current-time trace recorded at the working electrode in FIA.

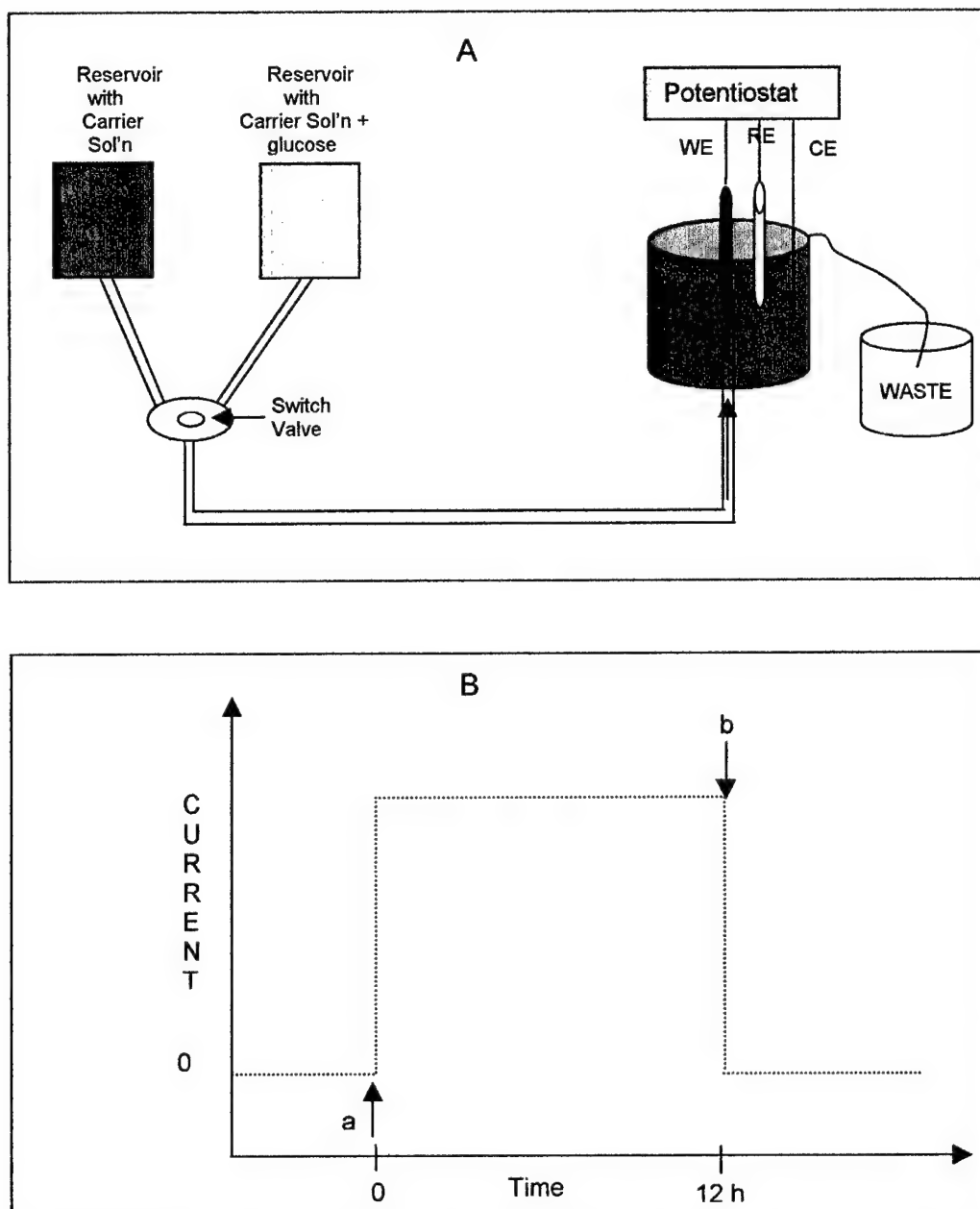


**Figure 9.** (A) Two-container flow system used to test the long-term operational stability of biosensors; (B) A schematic current-time trace recorded at the working electrode in the flow system. Arrows indicate the valve switch from background electrolyte reservoir to the analyte reservoir (a), and back to the background electrolyte (b).

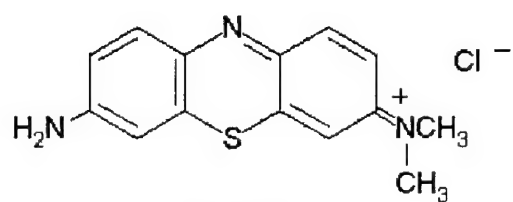
solution containing the analyte species. By switching from one reservoir to another, the analytical performance of the working electrode (biosensor) can be examined under the long exposure to the analyte species (Figure 8B).

### 1.3 RESULTS AND DISCUSSION

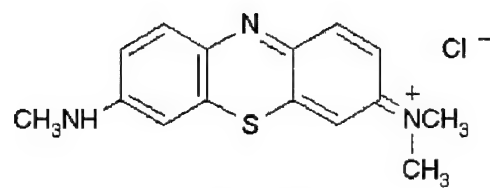
#### 1.3.1 Azure Dyes as Homogeneous Oxidants for Glucose Oxidase

Figure 10 shows the chemical structures of the azure dyes used in the present study. They contain three rings with heteroatoms N and S in the central ring. The redox process of azure dyes is depicted in Figure 11.

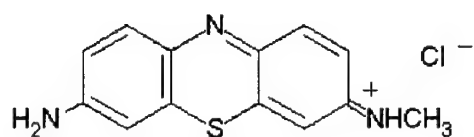
Figure 12 presents cyclic voltammograms recorded at a bare glassy carbon electrode in solutions containing Azure A + glucose (curve a), and Azure A + glucose + glucose oxidase (curve b). Figures 13 and 14 present the same voltametric data but for Azure B and Azure C, respectively. The voltammogram (a) in Figure 12 displays a pair of current peaks at a mid-peak potential of  $-0.220$  V, which is due to the redox of Azure A. The separation of current peaks is  $\sim 30$  mV, which is indicative of a two electron electrode process controlled by diffusion.<sup>35</sup> Glucose is not electroactive under these experimental conditions. The addition of GOx to the solution containing Azure A and glucose results in an S-shaped voltammogram (Figure 12, curve b).



Azure A



Azure B



Azure C

**Figure 10.** Structures of the azure dyes used in the present study.

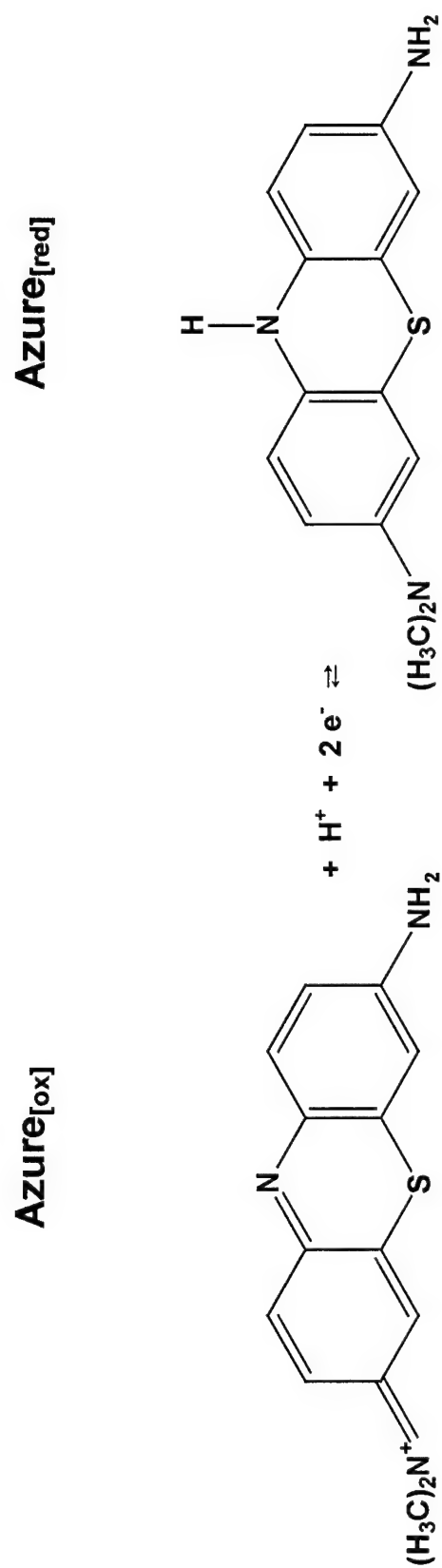


**Figure 11.** Redox of azure dyes exemplified with the Azure A species.

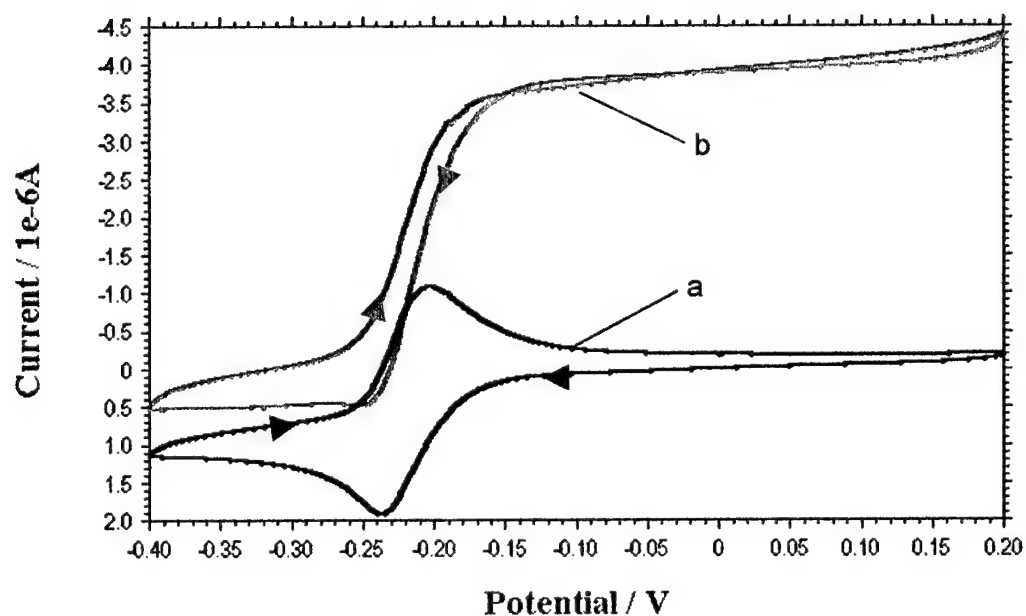


**Figure 12.** Cyclic voltammograms recorded at a bare glassy carbon electrode in a solution containing 0.50 mM Azure A + 50 mM glucose (a), and after the addition of 40  $\mu$ M GOx to the solution (b). Background electrolyte, pH 7.40 deoxygenated phosphate buffer. Scan rate, 1  $\text{mV s}^{-1}$ .

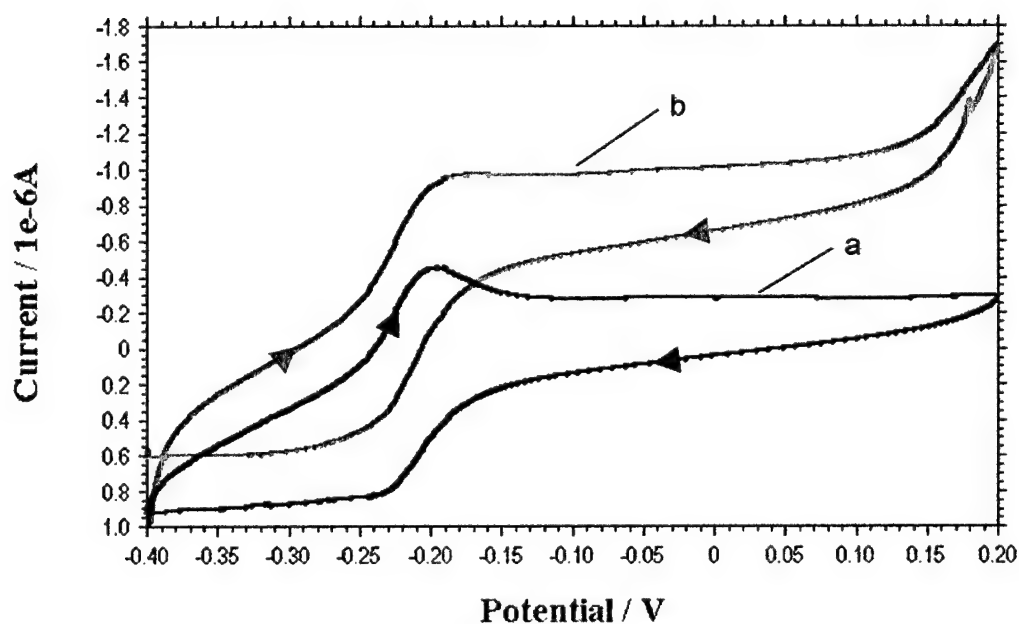


**Figure 13.** Cyclic voltammograms recorded at a bare glassy carbon electrode in a solution containing 0.10 mM Azure B + 50 mM glucose (a), and after the addition of 30  $\mu$ M GOx to the solution (b). Background electrolyte, pH 7.40 deoxygenated phosphate buffer. Scan rate, 2  $\text{mV s}^{-1}$ .

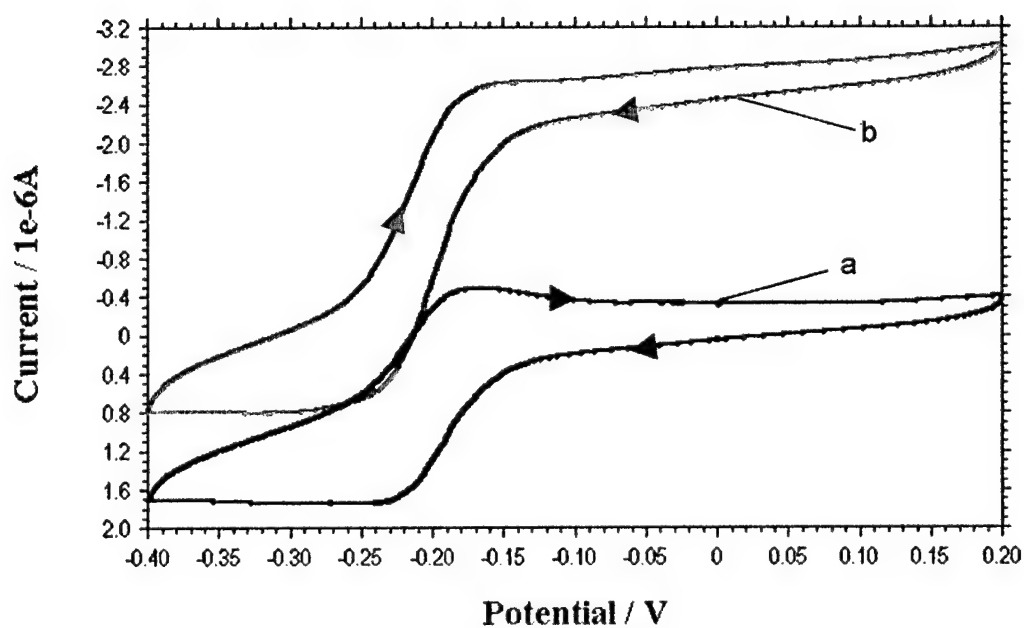


**Figure 14.** Cyclic voltammograms recorded at a bare glassy carbon electrode in a solution containing 0.50 mM Azure C + 50 mM glucose (a), and after the addition of 40  $\mu$ M GOx to the solution (b). Background electrolyte, pH 7.40 deoxygenated phosphate buffer. Scan rate, 5  $\text{mV s}^{-1}$ .

The following catalytic scheme describes the reaction sequence in the Azure mediated voltammetry of the enzymatic reaction



In this mechanism, the  $\text{Azure}_{\text{red}}$  species are generated (eq 5) in the presence of the reduced enzyme  $\text{GOx(FADH}_2\text{)}$ . The latter is maintained in the reduced state by the glucose substrate (eq 4). The oxidation of the  $\text{Azure}_{\text{red}}$  species at the electrode (eq 6) accounts for the enhanced anodic current seen on the S-shaped voltammograms in Figures 12-14.

The rate constant  $k$  of a homogeneous reaction between the reduced form of the enzyme, and azure dyes (eq 5) was determined by the analysis of the S-shaped voltammograms recorded in the excess of glucose to ensure that the enzyme is completely reduced. Under such condition, reaction (5) is pseudo-first-order, and the limiting current  $I_\infty$  due to redox mediation, can be described as<sup>12</sup>

$$I_\infty = nFAC_{\text{med}}(D_{\text{med}}kC_{\text{enz}})^{1/2} \quad (7)$$

where  $k$  is the rate constant of reaction (5),  $C_{\text{med}}$  and  $C_{\text{enz}}$  are the concentrations of the mediator and the reduced enzyme, respectively,  $D_{\text{med}}$  is the diffusion coefficient of the mediator, and the other symbols have the same meaning as in eq 3. A division of eq 7

by eq 3, which describes the diffusion-controlled current  $I_d$ , results in the expression for the current ratio

$$I_{\infty}/I_d = (kC_{enz})^{1/2}/[0.4463(nFv/RT)^{1/2}] \quad (8)$$

that contains easy to determine experimental parameters,  $I_{\infty}$  and  $I_d$ . The eq 8 is suitable in the present case, because the electrode process of the azure redox couple (eq 6) is controlled by diffusion. The rate constant  $k$  was calculated using the eq 8 and the voltammetric currents  $I_{\infty}$  and  $I_d$  that were recorded at slow scan rates (1 through 5  $\text{mV s}^{-1}$ ) in 0.5 mM Azure + 50 mM glucose solutions containing 0 – 40  $\mu\text{M}$  GOx. The rate constants obtained for the different mediators are presented in Table 1. A comparison of the rate constants indicates that the reactivity of azure dyes toward the oxidation of a reduced form of glucose oxidase increases in the order Azure B < Azure A < Azure C. This order corresponds with the decreasing number of methyl groups in the azure dye structures (Figure 10).

Table 1. Homogeneous rate constants for the reaction between azure dye and glucose oxidase (eq 5). The relative standard deviations are below 10 %.

Mediator	Rate Constant, $k$ ( $\text{M}^{-1}\text{s}^{-1}$ )
Azure B	1600
Azure A	4900
Azure C	8900

Apparently, the presence of methyl groups introduces steric hindrances that slow the electron transfer between the azure species and glucose oxidase. One can hypothesize that the bulkier the dye molecule the more difficult access it has to the FAD centers hidden within the enzyme.

The rate constants shown in Table 1 indicate that all of the azure dyes studied are quite rapid oxidants for glucose oxidase. Therefore they can be used as mediators for coupling the glucose oxidase/glucose system to an electrode surface in electrochemical glucose biosensors. Interestingly, Figures 12-14 show that such a coupling can be accomplished at low electrode potentials (e.g., 0 V). At such a low potential, the interferences from the redox active species that are commonly present in physiological samples of glucose can be avoided.

#### **1.4 CONCLUSIONS – PART 1**

Our cyclic voltammetric studies have shown that azure dyes are efficient redox mediators for the enzymatic reaction between glucose oxidase and glucose. The enzymatic reaction is mediated at low electrode potentials, which relate to the standard potentials of azure dyes. These properties suggest that azure dyes can be used as redox mediators in the design of fast and interference-free electrochemical biosensors based on glucose oxidase.

## **PART 2**

### **2.0 Immobilization of Azure Dyes and Glucose Oxidase on the Electrode Surface: A Reagentless Glucose Biosensor Design**

#### **2.0.1 Introduction**

By immobilizing both the redox mediators and enzymes on the electrode surface the reagentless biosensors can be realized. Such biosensors are convenient to use because they can operate in samples containing no enzymes or mediators. The immobilization of component species on the electrode surfaces has been accomplished, more or less successfully, by using a variety of methods, including, covalent bonding<sup>36-39</sup>, bioaffinity attachment<sup>40-42</sup>, entrapment in organic polymers<sup>43-46</sup>, redox gels<sup>47-49</sup>, sol-gel derived glasses<sup>50,51</sup>, carbon pastes<sup>52-54</sup>, and carbon-polymer electrodes.<sup>55,56</sup> However, even under the best conditions the majority of present-day reagentless biosensors display a limited operational stability. In other words, the more frequent use of a biosensor the faster its signal decays. This problem was traced to leaching of a mediator from the biosensor and enzyme inactivation in the biosensor. Apparently, the immobilization methods currently used, although preventing the enzyme from leaching, employ matrices that are not compatible enough with proteins to assure their sufficient protection in a biosensor.

After identifying the azure dyes as efficient homogeneous oxidants for glucose oxidase, we began to explore several synthetic approaches to immobilize them, and

glucose oxidase, on the electrode surface in order to prepare a reagentless glucose biosensor. The biopolymer chitosan was selected as the immobilization matrix.

Chitosan is a linear copolymer of glucosamine and N-acetylglucosamine units. It is obtained by the partial deacetylation of chitin. Chitin is a natural polymer made of N-acetylated glucosamine units, naturally found in the exoskeleton of crustaceans and fungi cell walls. When the degree of acetylation (expressed as molar percentage) is lower than 50%, chitosan becomes soluble in acidic solutions ( $\text{pH} < 6$ ) due to the protonation of its amino groups ( $\text{pK}_a$  6.3).<sup>57</sup> The chemical structures of chitosan and chitin are shown in Figure 15. Chitosan was chosen as the immobilization matrix because of its biocompatibility, non-toxicity, high mechanical strength, and excellent membrane forming ability.<sup>58</sup> In addition, chitosan possesses reactive hydroxyl and amino functional groups that can be used to covalently immobilize azure dyes.

Chitosan has been used previously for immobilization of various enzymes in bioreactors.<sup>59,60</sup> However, its applications for the development of electrochemical biosensors are very limited.<sup>61-64</sup>

## **2.1 Immobilization of Azure Dyes Within the Chitosan Matrix**

The synthetic approach to the immobilization of azure dyes relied on using bifunctional tethering molecules that can react with amino groups of chitosan (CHIT) and azure dyes. A conceptual representation of intended structures resulting from such a reaction is presented in Figure 16. After such CHIT-Tether-Azure structures were synthesized, they were mixed with a solution of enzyme glucose oxidase and cast on the electrode surface to form, after water evaporation, a biosensing film. The

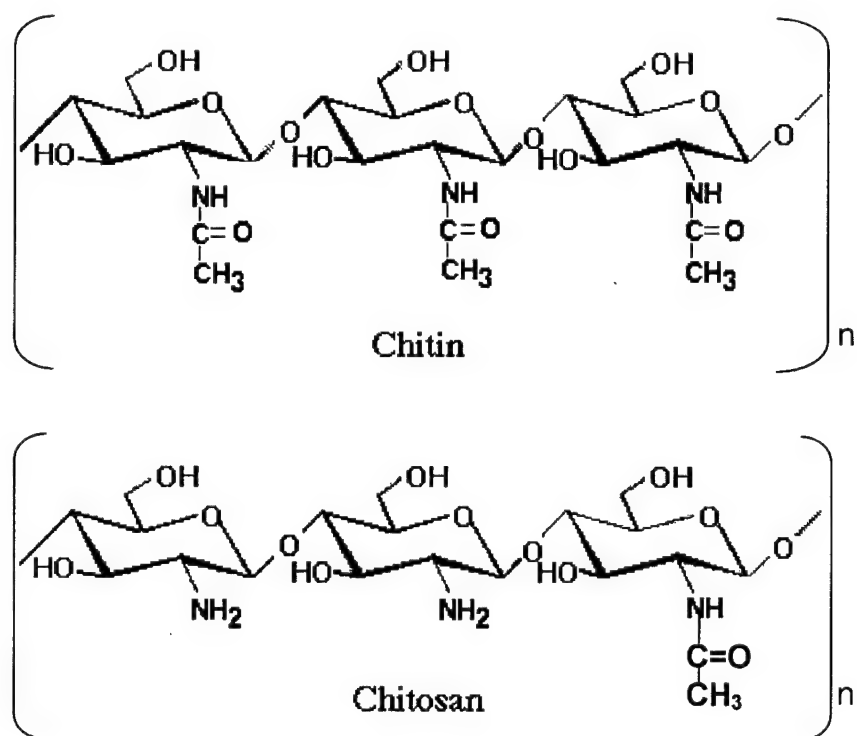


**Figure 15.** Structures of chitin and chitosan.

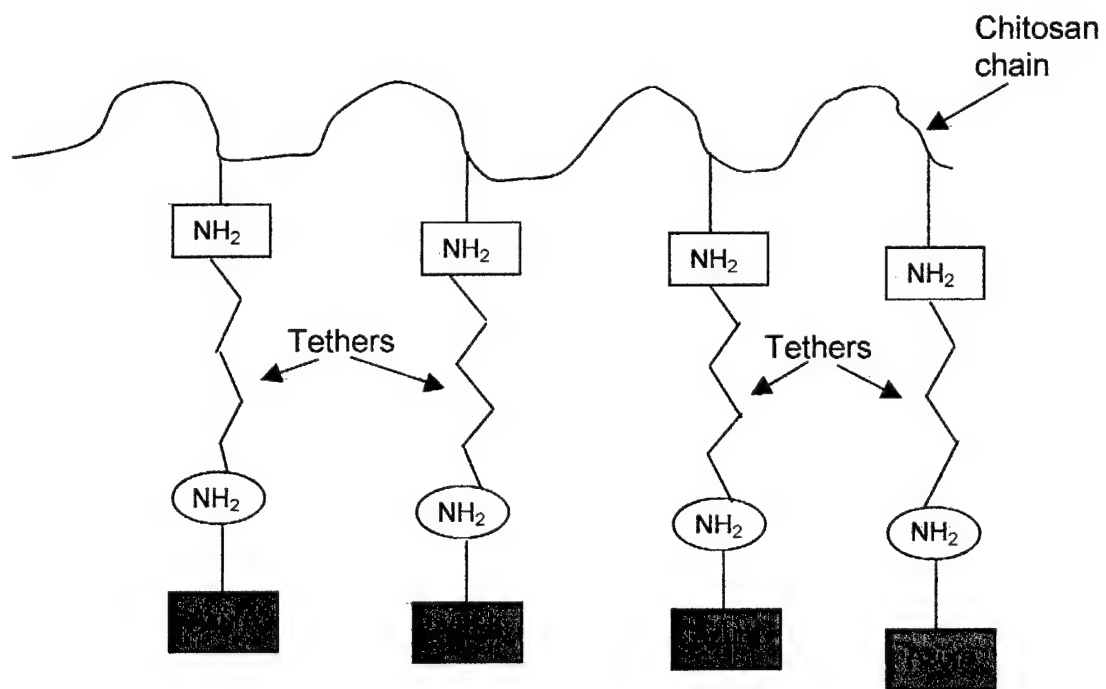
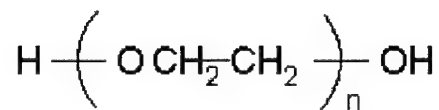


**Figure 16.** Schematic structure of the final product of the reaction CHIT + Tether + Azure.

length of tethering molecules was varied in order to optimize the efficiency of the immobilized azure dyes to mediate the electron transfer between the enzyme and electrode.

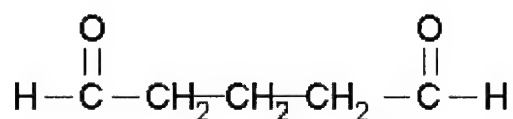
The chemical structures of tethers used in the present work are presented in Figure 17. They range from rather short carbon-chain molecules (e.g., acryloyl chloride) to very long ones (e.g., poly(ethylene glycol) and poly(ethylene glycol) diglycidyl ether). In addition, the tethers contain different functional groups that are reactive towards the amino groups of chitosan and azure dyes.

Figure 18 shows the chemistry of the tethering of azure molecules to chitosan using different tethers. Five tethering approaches were explored. The first approach A was based on the formation of Schiff-base structures by reacting the amino groups of chitosan and azure dye with the aldehyde groups of glutaric dialdehyde (GDI). This was accomplished in two steps. In the first step, solutions of chitosan and GDI were mixed and allowed to react for five hours at room temperature. A high molar ratio of GDI to chitosan glucosamine units (10:1 or 200:1) was used in order to ensure that only one aldehyde group of the GDI molecules was linked to amino groups of chitosan. The completion of the reaction was judged by an increase in solution viscosity that was accompanied by a change in color to yellow. The unreacted GDI molecules were removed from the reaction mixture by dialysis. In the second step, the product CHIT-GDI was reacted with a solution of azure for five hours in order to synthesize the CHIT-GDI-Azure product. The molar ratios of azure to chitosan glucosamine units were 1:1 or 2:1. The unreacted azure molecules were removed using extraction,

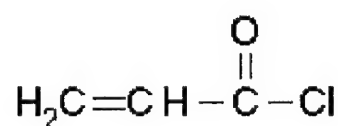


$$n \sim 600, 1000, 2000$$

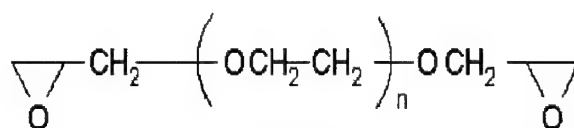
Poly(ethylene glycol) (PEG)



Glutaric dialdehyde (GDI)

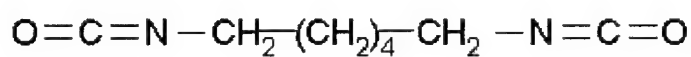


Acryloyl chloride (AcrCl)



$$n = 3 - 4$$

Poly(ethylene glycol) diglycidyl ether (PEGDGE)



Hexamethylene diisocyanate (HDI)

**Figure 17.** Structures of tethers used in the present study.

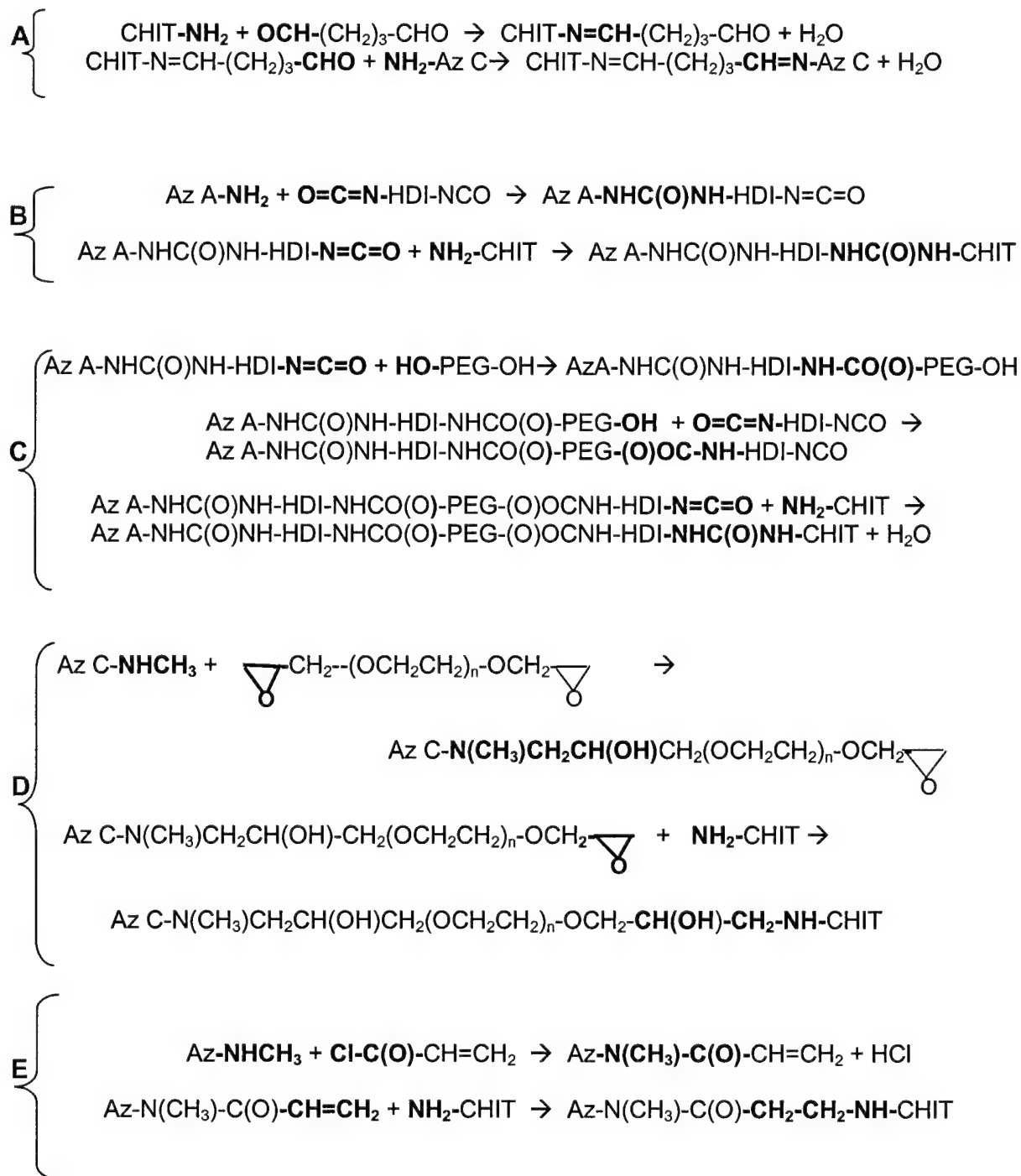


**Figure 18.** Chemical reactions between the chitosan (CHIT), tether molecule, and azure (Az) dye leading to the CHIT-tether-Az products.

dialysis or column chromatography. The reaction mixture (CHIT-GDI-Azure) after the separation step had a blue color, which is characteristic for azure dyes.

In the second approach B (Figure 18) a hexamethylene diisocyanate (HDI) was used as a tether. In order to react an amino group of azure A to an isocyanate group of HDI, the reaction between Azure A and HDI was carried out in dried dimethylformamide (DMF) at 85°C for one hour in the presence of the catalyst tin octoate. After cooling to room temperature, the solution of HDI-Azure A species was added slowly to a vigorously stirred solution of 0.5 wt. % chitosan in order to form the CHIT-HDI-Azure A product; the addition and mixing were continued until the molar ratio of Azure-HDI to glucosamine units of chitosan was equal to 1:1.

In order to extend the length of a tether (approach C in Figure 18), the Azure A-HDI species were reacted with poly(ethylene glycol) (PEG). The reaction between the Azure A-HDI and PEG (molar ratio 1:1) was carried out in DMF solution (60 °C, 1 h) containing tin octoate as a catalyst. The Azure-HDI-PEG species was subsequently reacted with an additional HDI to form the Azure-HDI-PEG-HDI product. In order to form the CHIT-HDI-PEG-HDI-Azure A structure, the solution containing the Azure-HDI-PEG-HDI was added slowly to a stirred solution of 0.5 (w/v) % chitosan until the reactants reached the molar ratio of 1:1.

The fourth approach to azure immobilization involved poly(ethylene glycol) diglycidyl ether (PEGDGE) as a tether (approach D in Figure 18). The amino groups of Azure C were reacted with the epoxide functionality of PEGDGE (molar ratio 2:1) under the following experimental conditions: Azure C dissolved in pH 7.40 phosphate buffer, was added to an aqueous solution of PEGDGE and stirred for three hours at

room temperature. The product Azure C-PEGDGE was then reacted with the aqueous solution of chitosan to yield CHIT-PEGDGE-Azure C species.

The fifth and last approach (Scheme E in Figure 18) relied on an acylation reaction using a hetero-functional tether acryloyl chloride (AcrCl). In this synthesis, the Azure B was dissolved in tetrahydrofuran (THF) containing 1,4-benzoquinone as a radical inhibitor. This was done in a tightly sealed glass vial under argon to prevent the moisture in the air from reacting with the components. Subsequently, a stoichiometric amount of acryloyl chloride was added dropwise through the septum using a syringe. The final molar ratio of amine groups to AcrCl was 2:1. After stirring the reaction mixture for six hours, the vial was opened and the THF was evaporated at room temperature. The resulting solid was dissolved in water and mixed with a solution of chitosan in order to form CHIT-AcrCl-Azure B product.

The presence of azure dyes in the final products was confirmed by UV-visible spectroscopy. However, the attempts to use FT-IR and NMR spectroscopies to confirm structures of the final products were inconclusive/unsuccessful. Therefore, the efficiency of azure immobilization on chitosan was studied using an electrochemical method, cyclic voltammetry. This method can be viewed as an ultimate test because it shows directly the level of mediation activity of the synthesized CHIT-Tether-Azure structures toward the enzymatic reaction.

## 2.2 RESULTS AND DISCUSSION

### 2.2.1 Electrochemical Testing of the Chitosan-Tether-Azure-GOx Films

In order to test the Chitosan-Tether-Azure products for enzyme mediation activity, the solutions were mixed with a solution of glucose oxidase and cast on the surface of glassy carbon electrode. In each case a robust surface film was formed after the water was evaporated. The film electrodes were immersed in pH 7.40 phosphate buffer solution and cyclic voltammograms were recorded.

In theory, such voltammograms should display a pair of current peaks due to the redox active azure molecules immobilized in the surface film. The peaks should be centered at  $\sim -0.220$  V, which is the standard potential of the  $\text{azure}_{\text{ox}}/\text{aure}_{\text{red}}$  redox couple. In addition, in the presence of glucose in the solution, the voltammograms should display an enhanced anodic current on the positive-going voltammetric scan. The origin of this current was explained earlier (eqs 4 – 6) in the case of the homogeneous kinetics study. In the present case, the enzyme and mediator are immobilized in the surface film instead of being dissolved in the solution. Figure 19 shows the mechanism of the redox mediation that should operate in the surface film. The presence of glucose in the solution should trigger the catalytic loops that ultimately generate a constant supply of the reduced form of azure. The oxidation of the reduced azure on the electrode surface is responsible for the enhanced anodic current that should be observed on the voltammograms.

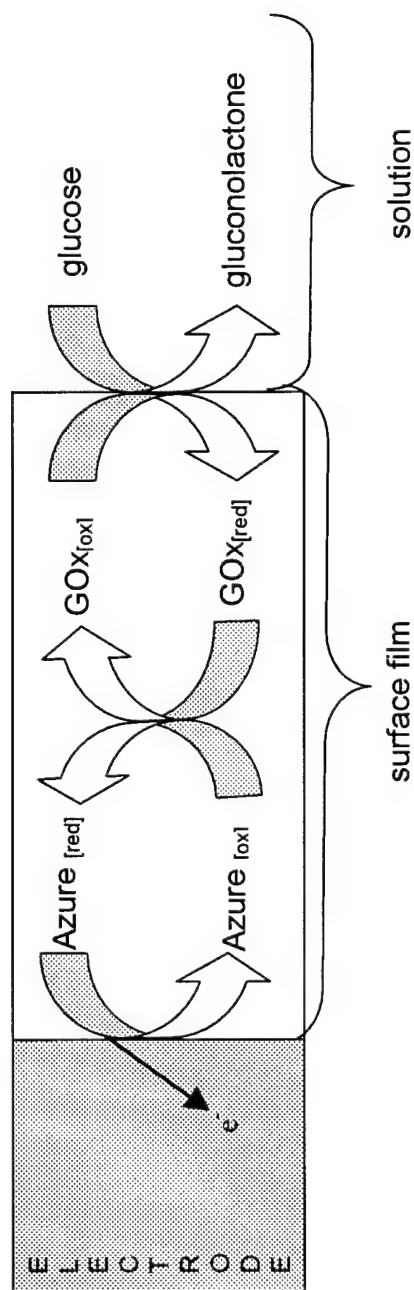


**Figure 19.** The mechanism of redox mediation in the biosensor based on a surface film. Glucose is oxidized to gluconolactone by the enzyme glucose oxidase. This reaction generates the reduced form of the enzyme,  $GOx_{[red]}$ . The mediator  $Azure_{[ox]}$  reoxidizes the  $GOx_{[red]}$  back to  $GOx_{[ox]}$  species, which is now ready to oxidize the next molecule of glucose. In this process, the mediator is reduced to the  $Azure_{[red]}$ . Finally, the  $Azure_{[red]}$  is re-oxidized at the electrode generating the flow of electrons (current). The current is proportional to the concentration of glucose in the solution. At high glucose concentrations the current levels off due to enzyme saturation.

Let us now compare the foregoing theoretical description of a biosensor action with experimental voltammetric results that were obtained using the five film electrodes (Figures 20 – 24). The voltammograms recorded at the electrodes coated with CHIT-AcrCl-AzB-GOx film (approach E) in phosphate buffer solution showed virtually no current peaks due to the redox of Azure B (Figure 20). Furthermore, the addition of glucose to the solution did not generate any extra current on the positive-going scan at  $E > 0$  V. Such a behavior indicates that the biosensing mechanism shown in Figure 19 does not operate in the CHIT-AcrCl-AzB-GOx film. Apparently, the acryloyl chloride tether is too short for the efficient electrical communication between azure mediator and electrode, and between azure and the FAD sites hidden inside the enzyme molecules.

Similar behavior was observed in the case of the electrode coated with the CHIT-PEGDGE-AzC-GOx film (approach D). Again, no current peaks due to the azure redox couple and no extra current in the presence of glucose were observed (Figure 21). This was rather a surprising result because the longer PEGDGE tether was expected to allow for an easy access of the Azure C, the fastest mediator in homogeneous studies, to the FAD site of the enzyme, as well as to the electrode surface. The small current obtained ( $\sim 10^{-7}$  A) indicates that either there is not enough azure dye in the film to do the mediation or the film does not allow for a fast ion transport. Thus, a small yield of mediator immobilization in chitosan seems to be responsible for the failure of this approach.

The CHIT-GDI-AzC-GOx film (approach A) is the first one that displays some of the expected biosensing behavior (Figure 22). The current peaks due to the redox of

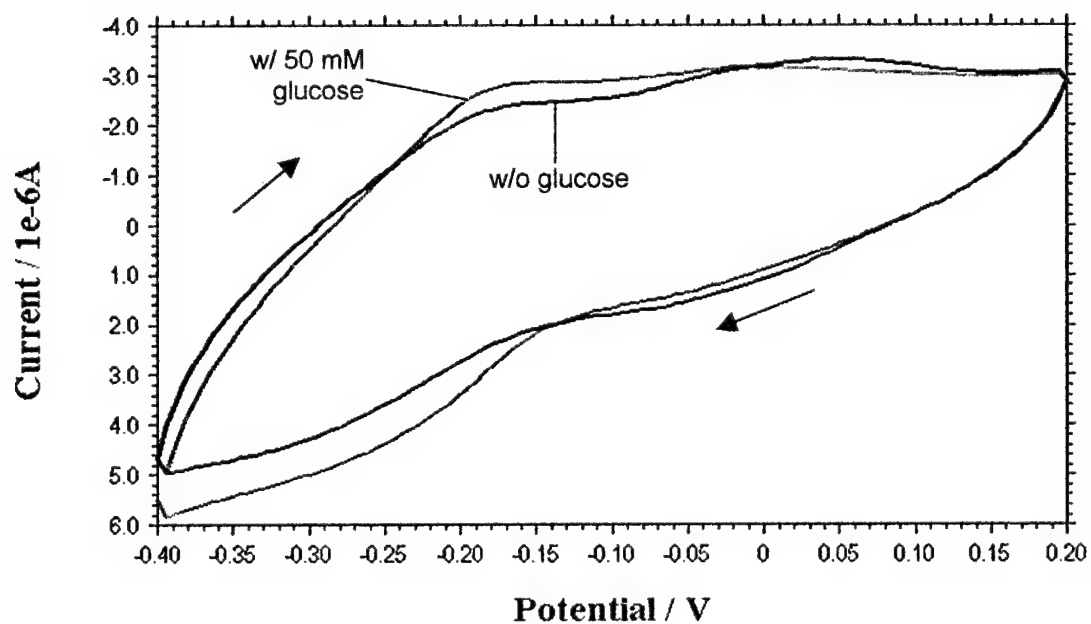


**Figure 20.** Cyclic voltammograms recorded at an electrode coated with the CHIT-AcrCl-AzB-GOx film (approach E). Background electrolyte, pH 7.40 deoxygenated phosphate buffer. Scan rate,  $50 \text{ mV s}^{-1}$ .

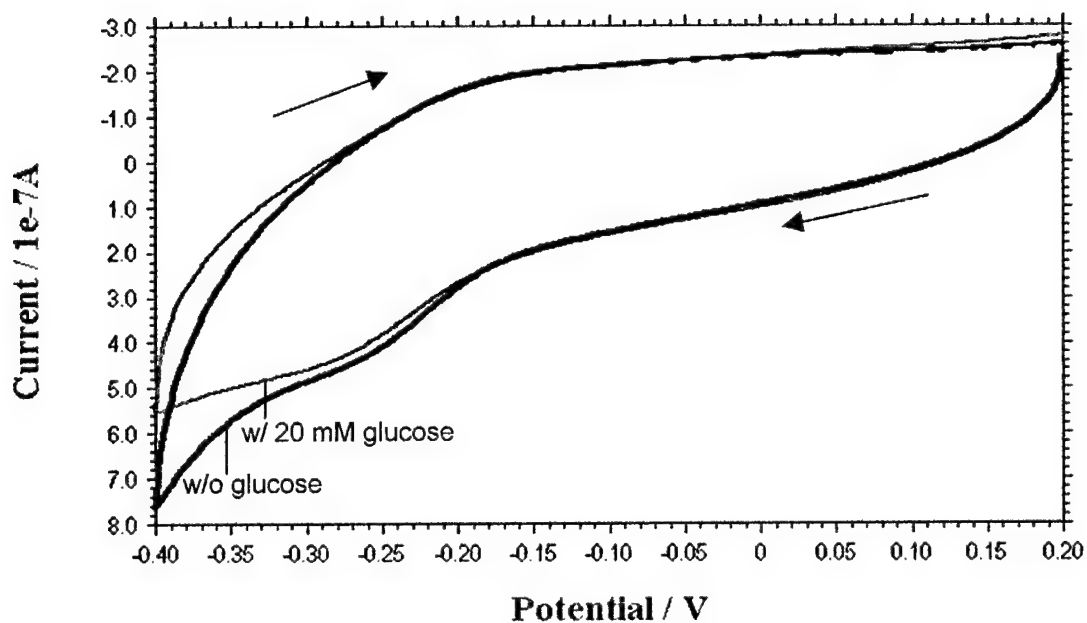


**Figure 21.** Cyclic voltammograms recorded at an electrode coated with the CHIT-PEGDGE-AzC-GOx film (approach D). Background electrolyte, pH 7.40 deoxygenated phosphate buffer. Scan rate,  $50 \text{ mV s}^{-1}$ .

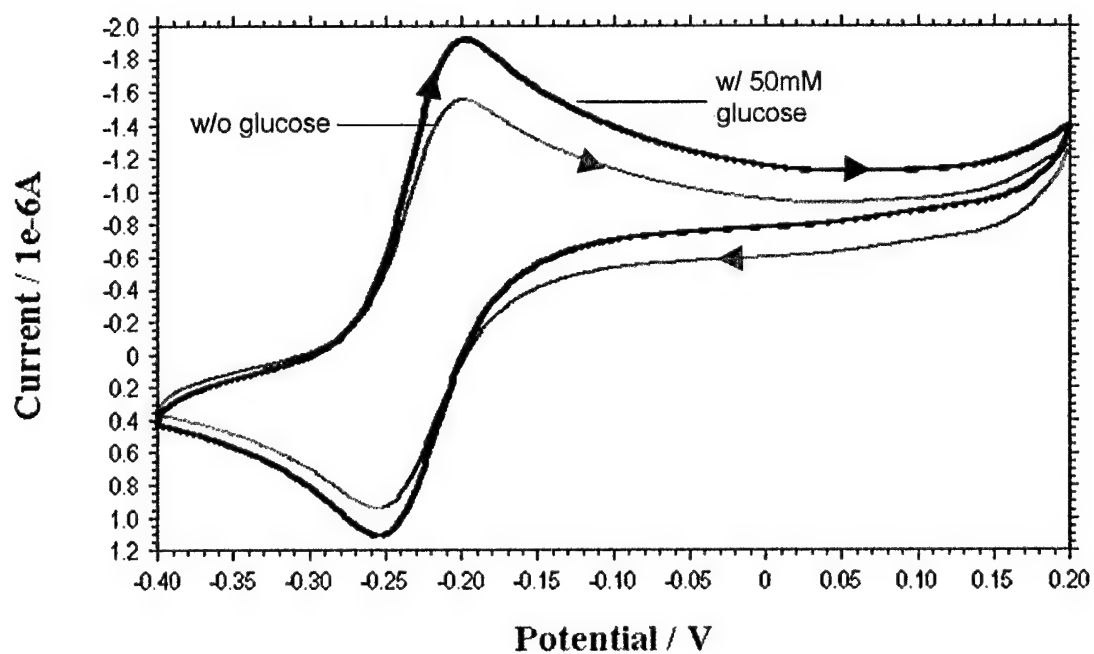


**Figure 22.** Cyclic voltammograms recorded at an electrode coated with the CHIT-GDI-AzC-GOx film (approach A). Background electrolyte, pH 7.40 deoxygenated phosphate buffer. Scan rate,  $10 \text{ mV s}^{-1}$ .

azure species in the film are well developed at mid-peak potential  $E = -0.220$  V, and the anodic current on the positive-going scan increases upon the addition of glucose to the solution. The peak separation of 50 mV is larger than the theoretical 30 mV (at 25°C) predicted for the two-electron process. This is indicative of the increased resistivity (ohmic drop) inside the surface film. Nevertheless, the existence of current peaks on the voltammograms indicates that the Azure C effectively communicates with the electrode surface. However, its electrical communication with the enzyme is limited as indicated by a rather small current increase in the presence of glucose. Apparently, the synthetic approach A results in a good yield for the azure immobilization, which allows for the large currents in the range of  $10^{-6}$  A, but the GDI tether seems to be too short for effective communication between the mediator and enzyme.

The most successful approaches to the immobilization of azure dyes on chitosan were those based on the use of HDI as a tether. Figure 23 shows voltammograms recorded at the electrode coated with the CHIT-HDI-AzA-GOx film (approach B). The currents due to the redox of azure species are large ( $I_d \cong 8 \mu\text{A}$ ) and the addition of glucose to the solution generates a substantial increase in the anodic current ( $I_{\infty} \cong 6 \mu\text{A}$ ). The kinetic parameter  $I_{\infty}/I_d$  is equal to  $\sim 0.75$ , which indicates a respectable mediation efficiency.

Even better kinetics of mediation were obtained with the CHIT-HDI-PEG-HDI-AzA film (approach C). Here the current ratio  $I_{\infty}/I_d$  is equal to  $\sim 1.0$  (Figure 24). The

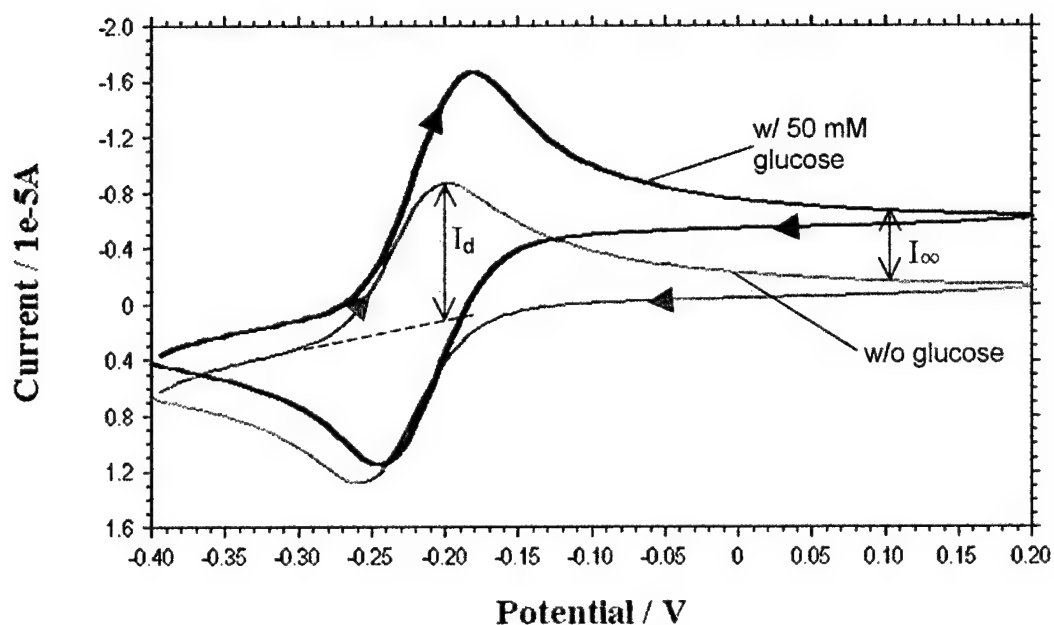


**Figure 23.** Cyclic voltammograms recorded at an electrode coated with the CHIT-HDI-AzA-GOx film (approach B). Background electrolyte, pH 7.40 deoxygenated phosphate buffer. Scan rate,  $30 \text{ mV s}^{-1}$ .

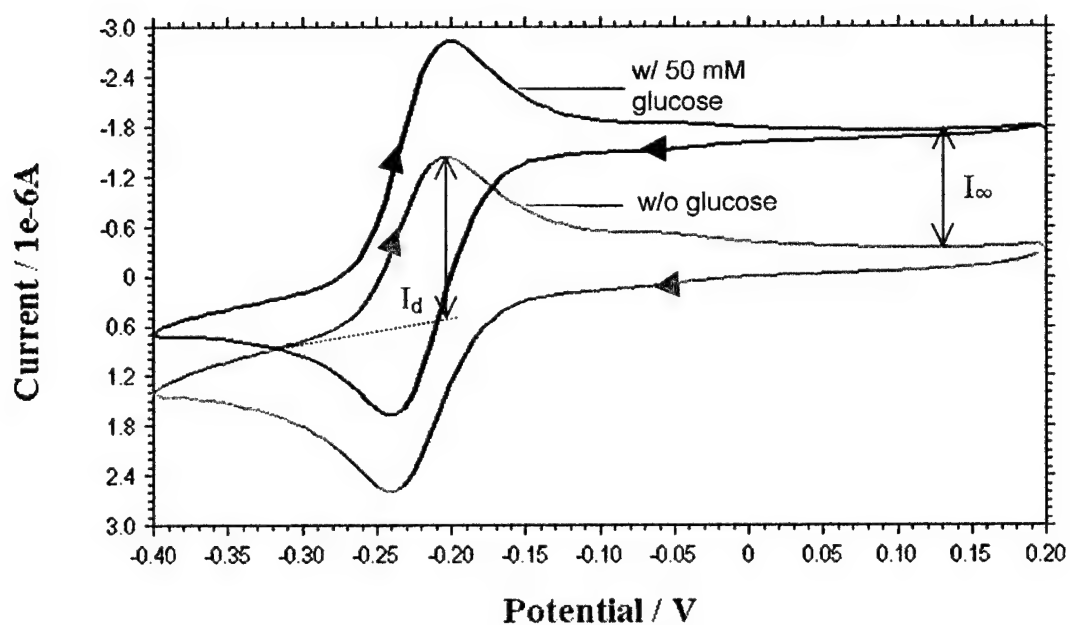


**Figure 24.** Cyclic voltammograms recorded at an electrode coated with the CHIT-HDI-PEG-HDI-AzA-Gox film (approach C). Background electrolyte, pH 7.40 deoxygenated phosphate buffer. Scan rate,  $60 \text{ mV s}^{-1}$ .

azure peak currents ( $I_d \cong 1.4 \mu\text{A}$ ) are smaller than those recorded at the CHIT-HDI-AzA-GOx film. This indicates a lower immobilization yield in approach C than in the less elaborate approach B. However, approach C uses a longer tether (HDI-PEG-HDI), which allows for more diffusional movement of azure mediator, permitting better electrical communication with the enzyme.

Such a voltammetric characteristic is very promising for the development of reagentless glucose biosensors based on the azure dyes immobilized together with enzymes in chitosan films. However, before any practical implementation of this concept can be made, more studies are required in order to solve some of the remaining problems that were detected in this study. One of them is a limited stability of such films caused by leaching of the modified chitosan chains from the electrode surface into the solution. A crosslinking of chitosan chains should alleviate this problem. Another difficulty is a slow response time of the film electrodes to glucose. In the batch experiments, the response times  $t_{90\%}$  (the time to reach 90 % of the signal) were on the order of several minutes to several dozen minutes. Currently, two strategies to shorten the response time are explored. They rely on using thinner surface films and lower molecular weight chitosan in order to speed up the mass transport to the electrode surface.

## 2.3 CONCLUSIONS – PART 2

This proof-of-concept study proved the feasibility of the biosensor design based on immobilization of enzymes and redox mediators in the matrix of the biopolymer chitosan (CHIT) on an electrode surface. The azure dyes (Az) can be immobilized within the chitosan matrix using bifunctional tethering molecules. In order to achieve an efficient redox mediation of an enzymatic reaction of glucose oxidase (GOx), the length of the tether has to be optimized. Out of the five synthetic approaches to the azure immobilization, the one based on the hexamethylene diisocyanate (HDI) tether was found to be the most efficient. The electrodes coated with either the CHIT-HDI-Az-GOx or CHIT-HDI-PEG-HDI-Az-GOx films displayed the best voltammetric characteristics for future biosensor applications. Future research on such biosensing systems should focus primarily on the improvement of the film stability and its response time to enzyme substrates.

## **PART 3**

### **3.0 Paste Enzyme Electrode Based on Azure Eosinate Mediator**

#### **3.0.1 Introduction**

Part 3 of this thesis was devoted to the integration of the enzyme glucose oxidase and azure mediators within the electron conductive paste. The carbon paste electrode, made of a mixture of carbon powder and a liquid nonelectroactive binder (oil), was invented by Ralph Adams in 1958.<sup>65</sup> The history of the paste electrode is very interesting and inspiring. It started with the idea to develop a “dropping carbon electrode” as a mimic of the dropping mercury electrode invented by Jaroslav Heyrovsky, who received the Nobel Prize for the development of polarography with dropping mercury electrodes. Adams’ original intention was to use the dropping carbon electrode for anodic oxidations of organic compounds where mercury electrodes were inapplicable. The experiments with carbon dropping electrodes failed. However, the concept of a stationary carbon paste electrode opened the whole new research area in electrochemistry. The research with carbon paste-based electrodes is documented in over 1000 publications, with approximately 50 – 100 manuscripts published annually in the past five years.<sup>66</sup> The milestones in the development of carbon paste electrodes include the chemical modifications of the paste with redox active species<sup>67</sup>, electrolytic binders<sup>68</sup>, complexing agents<sup>69</sup>, and biomolecules.<sup>70</sup> The

main advantages of carbon paste electrodes are the low cost, the ease of construction in different configurations and sizes, and the capability of adding large amounts of modifiers to the electrode. In addition, such electrodes have an easily renewable surface and display low background currents, which is important in analytical applications. The drawbacks of paste electrodes are the limited mechanical stability under hydrodynamic conditions and susceptibility to dissolution in some organic solvents. The advantages of using carbon paste as a matrix for the immobilization of enzymes surpass its drawbacks if such electrodes are used to analyze aqueous samples, which is the goal of the present study.

In this part of the thesis, the glucose biosensor based on the paste electrode is described. The carbon paste was modified by adding the enzyme glucose oxidase and a sparingly soluble redox mediator, azure eosinate. Our hypothesis was that such a sparingly soluble salt of azure, when assembled together with glucose oxidase in the matrix of carbon paste, would act as a source of azure species for the enzyme reoxidation according to eq 5. Since azure species are not covalently immobilized in the paste, it was expected that they would have an easy access to the FAD centers of the enzyme and, thus, provide a faster response time of a biosensor to glucose.

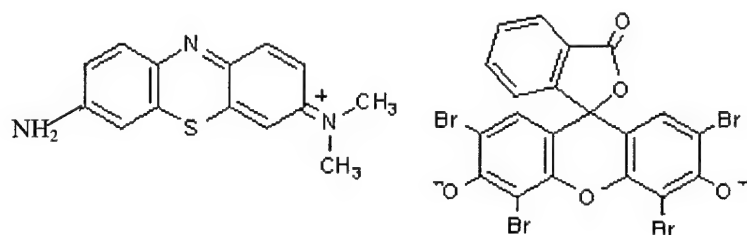
### 3.1 RESULTS AND DISCUSSION

#### 3.1.1 Azure Eosinate Dyes as Homogenous Oxidants for Glucose Oxidase

Prior to incorporating the azure eosinates (Figure 25) into the carbon paste, their capability to mediate the enzymatic reaction was investigated. To this end, the homogeneous kinetics of the reaction



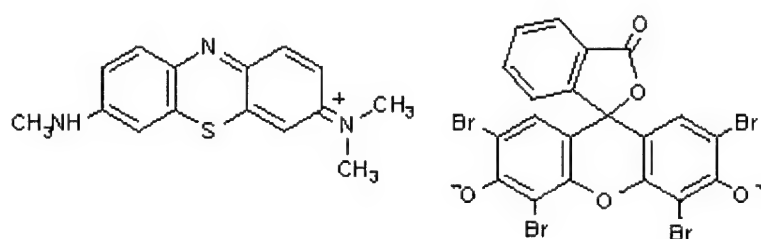
was determined. The solutions for the kinetic studies were prepared by overnight equilibration of azure eosinate in pH 7.40 phosphate buffer. The solutions were centrifuged to remove the solid azure eosinate that did not dissolve. To such solutions, the glucose and glucose oxidase were added and the cyclic voltammograms at the bare glassy carbon electrodes were recorded. Figure 26 shows such voltammograms obtained with Azure A Eosinate as a mediator. The voltammogram recorded in the presence of glucose and enzyme in the solution displays a distinctly enhanced anodic current (at  $E > -0.2$  V) due to the redox mediation. The Azure B Eosinate shows a similar redox mediation capability (Figure 27). The currents recorded in the Azure B Eosinate system are larger because of a better solubility of Azure B Eosinate ( $2 \text{ mg mL}^{-1}$ ) than of Azure A Eosinate ( $1 \text{ mg mL}^{-1}$ ). Interestingly, at potentials more positive than  $\sim 0.2$  V, a second redox mediation system is observed as indicated by the further increase in the anodic current (Figures 26 and 27). However,



Azure A

Eosinate

Azure : Eosinate  
2 : 1



Azure B

Eosinate

Azure : Eosinate  
2 : 1

**Figure 25.** Structures of Azure A Eosinate (top) and Azure B Eosinates (bottom).

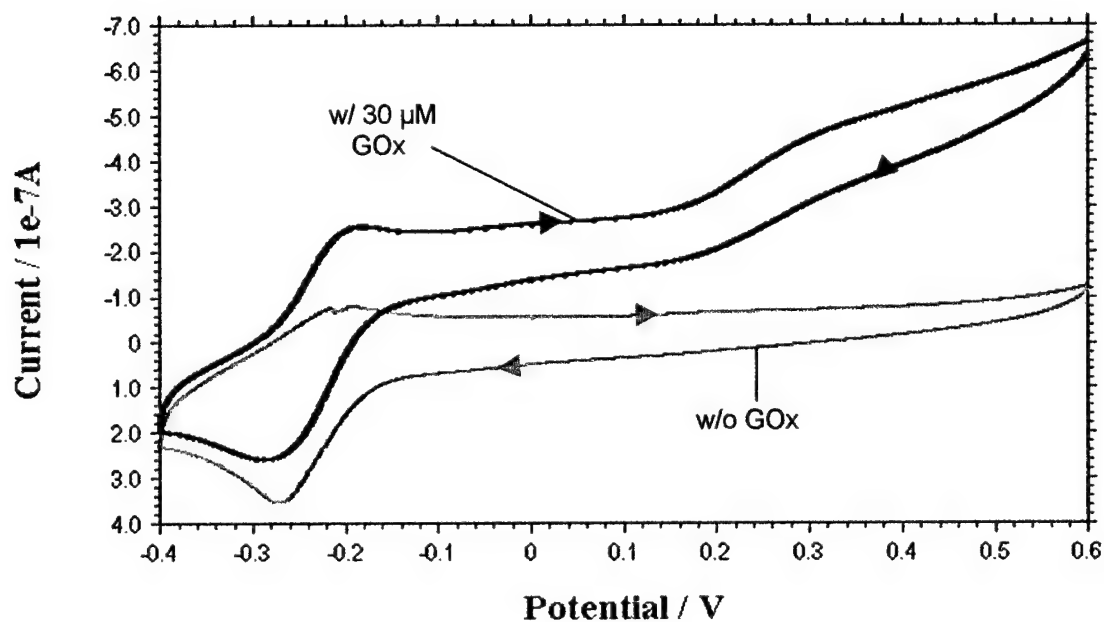


**Figure 26.** Cyclic voltammograms recorded at a bare glassy carbon electrode in Azure A Eosinate + 50 mM glucose solution under argon. Background electrolyte, pH 7.40 phosphate buffer. Scan rate,  $2 \text{ mV s}^{-1}$ .

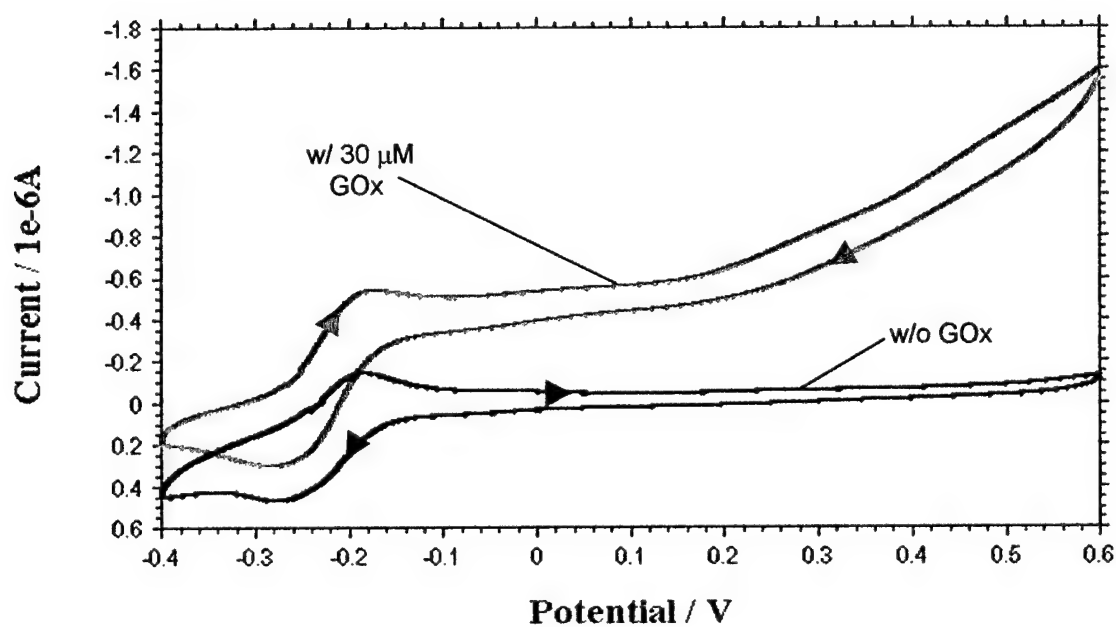


**Figure 27.** Cyclic voltammograms recorded at a bare glassy carbon electrode in Azure B Eosinate + 50 mM glucose solution under argon. Background electrolyte, pH 7.40 phosphate buffer. Scan rate,  $2 \text{ mV s}^{-1}$ .

our focus was on the first mediation, which is seen in the potential range between  $-0.2$  V and  $+0.2$  V. The rationale was that at lower potentials the sensing of glucose should be less prone to interferences from redox active species other than glucose.

The rate constant  $k$  of a reaction (9) was calculated using the voltammograms shown in Figures 26 and 27, and following the procedure described in Part 1 (eq 8). The rate constants were found to be equal to  $600$  and  $1,700 \text{ M}^{-1} \text{ s}^{-1}$  for Azure A Eosinate and Azure B Eosinate, respectively. Thus, the Azure B Eosinate is a faster mediator than the Azure A Eosinate. This kinetic order is different from that found in Part I, which showed that Azure A chloride was a faster mediator than the Azure B chloride. In addition, generally, the rate constants for the azure eosinates are smaller than those for azure chlorides (Table 1). Apparently, the bulky eosinate anion modifies the reactivity of the azure cation. The ion pairing between the azure cation and eosinate is probably responsible for this effect. One can hypothesize that the anionic and bulky [azure–eosinate] $^{-}$  ion pairs have more limited access to the FAD sites of the negatively charged glucose oxidase than the azure cations originating from the dissociation of azure chlorides.

### **3.1.2 Paste Azure Eosinate A Glucose Oxidase Electrodes as Biosensors for Glucose**

The paste electrodes were prepared using Azure A Eosinate as a mediator even though it is a slower mediator than the Azure B Eosinate. The rationale was that the more hydrophobic Azure A Eosinate should be better retained in the carbon-oil

paste than the more soluble Azure B Eosinate. This was indeed the case, and our study showed that the Azure A Eosinate-based paste biosensor retained its activity toward glucose for extended periods of time (at least several weeks).

The paste electrodes containing 25 wt. % of enzyme and either 28 or 40 wt. % of Azure A Eosinate were investigated as biosensors for glucose. This comparative study involved electrochemical techniques such as cyclic voltammetry, chronoamperometry in stirred solutions, chronoamperometry in a flow system, and flow injection analysis.

Figures 28 and 29 show cyclic voltammograms recorded at the paste electrodes in the absence and presence of glucose in the solution. In the presence of glucose the increased anodic currents were observed at potentials more positive than  $-0.2$  V. This indicated that the mediation mechanism shown in Figure 19 does operate in the pastes. The currents recorded at the paste electrode containing 28 wt. % Azure A Eosinate were approximately an order of magnitude larger than those obtained with the electrode having 40 wt. % Azure A Eosinate. This rather unexpected behavior is probably a result of either a partial deactivation of enzyme by the mediator or a limited accessibility of glucose to enzyme in the paste with a higher content of Azure A Eosinate. The alternative explanation would be that the lower currents at the 40 wt. % - paste electrode are due to the lower content of carbon powder, which is the only electron-conducting component of the paste. However, the peak potentials seen in Figures 28 and 29 are practically the same ( $\sim 0.190 - 0.180$  V), which indicates no difference in the electrical resistivity of the two pastes.

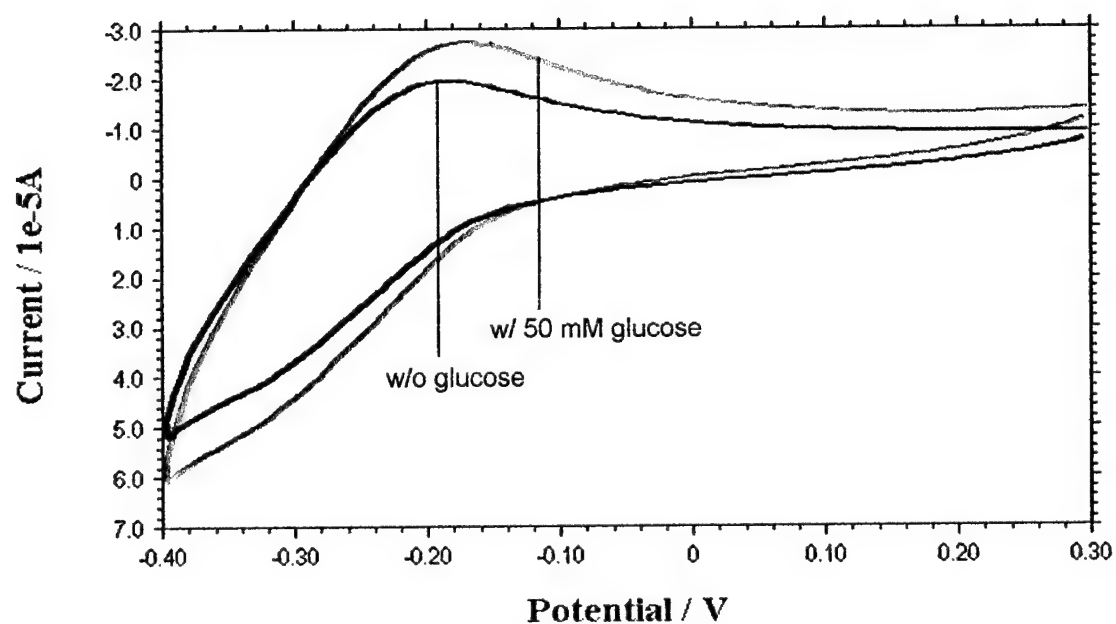


**Figure 28.** Cyclic voltammograms recorded at a paste electrode containing 28 wt % Azure A Eosinate. Background electrolyte, pH 7.40 phosphate buffer deoxygenated with argon. Scan rate,  $10 \text{ mV s}^{-1}$ .

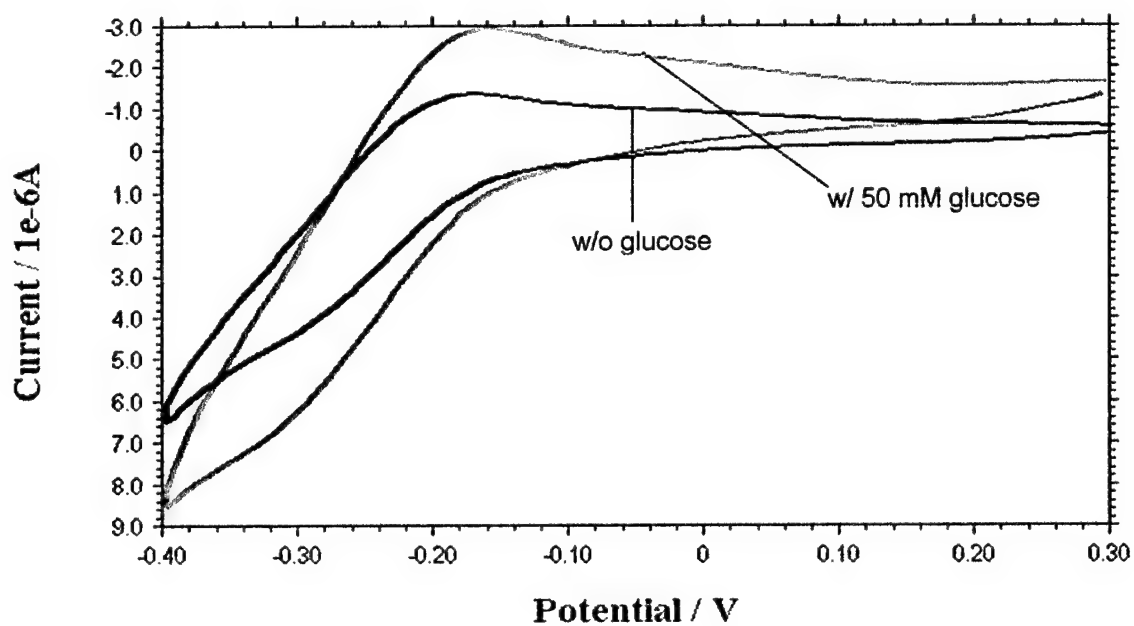
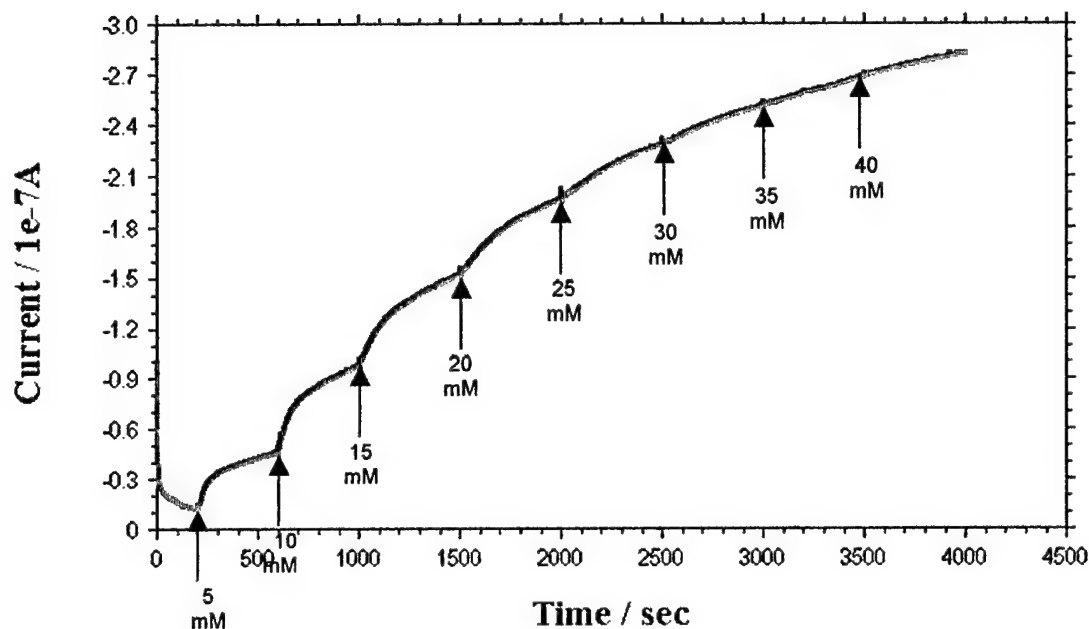


**Figure 29.** Cyclic voltammograms recorded at a paste electrode containing 40 wt % Azure A Eosinate. Background electrolyte, pH 7.40 phosphate buffer deoxygenated with argon. Scan rate,  $10 \text{ mV s}^{-1}$ .

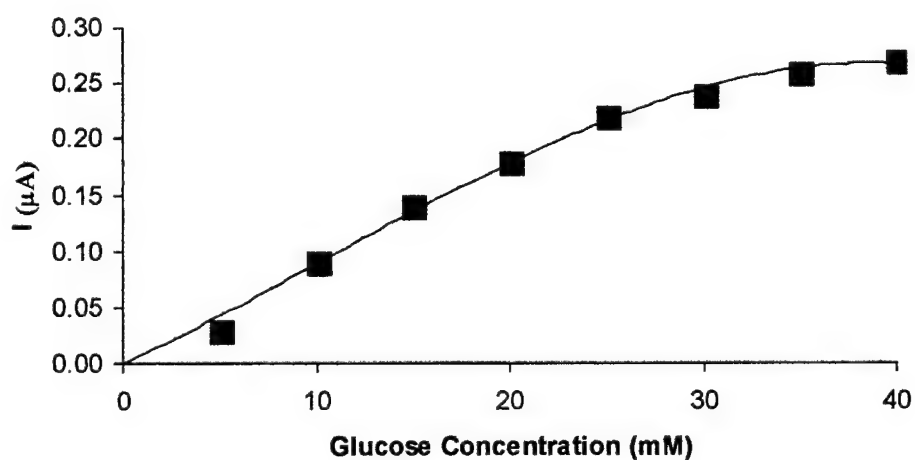
Figure 30 presents an amperometric trace obtained at the 28 wt. % paste electrode in a stirred solution that was spiked with increasing amount of glucose ("batch experiment"). The electrode responds quickly ( $t_{90\%} \leq 2$  min) to the changing concentrations of glucose at  $C_{\text{glucose}} < 25$  mM. The calibration plot for glucose, shown in Figure 31, indicates that the linear range of this biosensor is from 3 to 25 mM glucose, which covers the physiologically important range of glucose concentrations in blood. Similar analysis of the paste electrode containing 40 wt. % Azure A Eosinate (Figures 32 and 33) indicates that this electrode is less sensitive to glucose and displays a more narrow linear range ( $<15$  mM glucose).

Figure 34 shows the flow injection analysis (FIA) of glucose performed with the paste electrode containing 28 wt. % Azure A Eosinate. Under such conditions, the linear range of the electrode is smaller than that observed in the batch experiment. The analogous analysis carried out with the electrode having 40 wt. % Azure A Eosinate showed a severe limitation at glucose concentrations larger than 13 mM (Figure 35). A decrease in the height of FIA peaks at  $C_{\text{glucose}} > 13$  mM is caused by a slow response time of the biosensor. In the FIA experiment, the biosensor is exposed to a plug of the injected glucose for only a few seconds. This short residence time, when combined with a slow response time at larger glucose concentrations, results in a decrease of the signal at  $C_{\text{glucose}} > 13$  mM.

Figure 36 shows an amperometric response of the paste electrode (28 wt. % Azure A Eosinate) to 5 mM glucose, which is an average glucose concentration in non-diabetic blood samples, and to several potential interfering species at concentrations close to their relevant clinical levels. Because the electrode operates



**Figure 30.** Chronoamperogram recorded at a paste electrode containing 28 wt. % Azure A Eosinate. The arrows indicate the additions of glucose stock solution to a stirred solution of phosphate buffer, pH 7.40. Potential, 0.0 V.



**Figure 31.** Calibration plot for glucose constructed using the data in Figure 30.

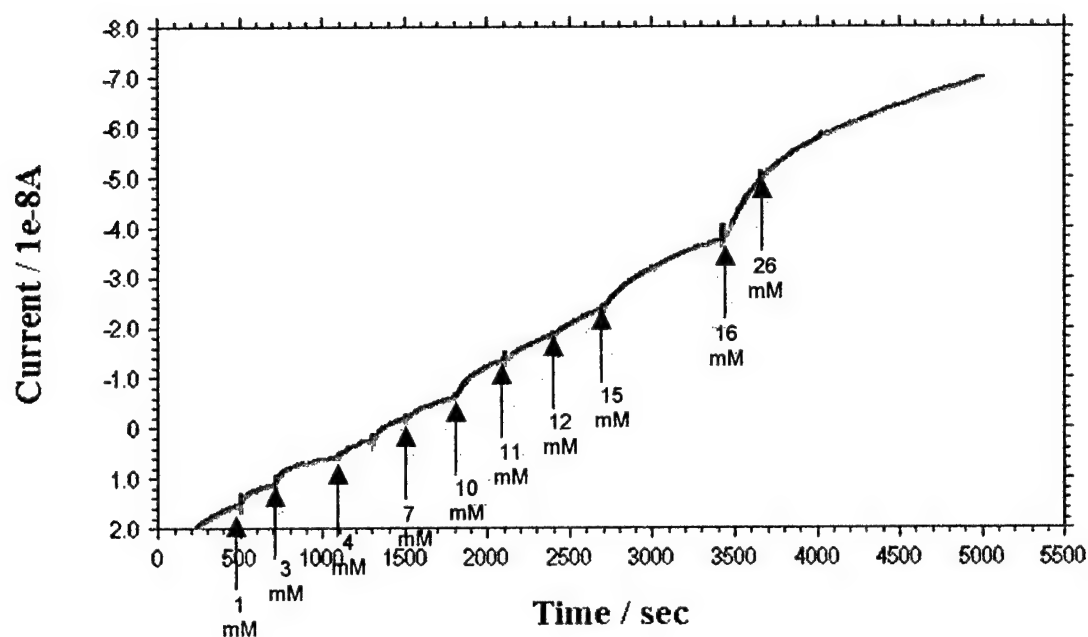


**Figure 32.** Chronoamperogram recorded at a paste electrode containing 40 wt. % Azure A Eosinate. The arrows indicate the additions of glucose stock solution to a stirred solution of phosphate buffer, pH 7.40. Potential, 0.0 V.

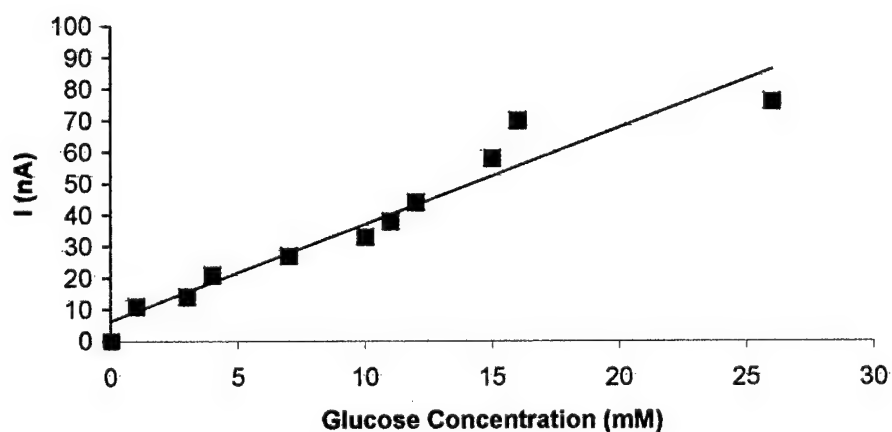


**Figure 33.** Calibration plot for glucose constructed using the data in Figure 32.

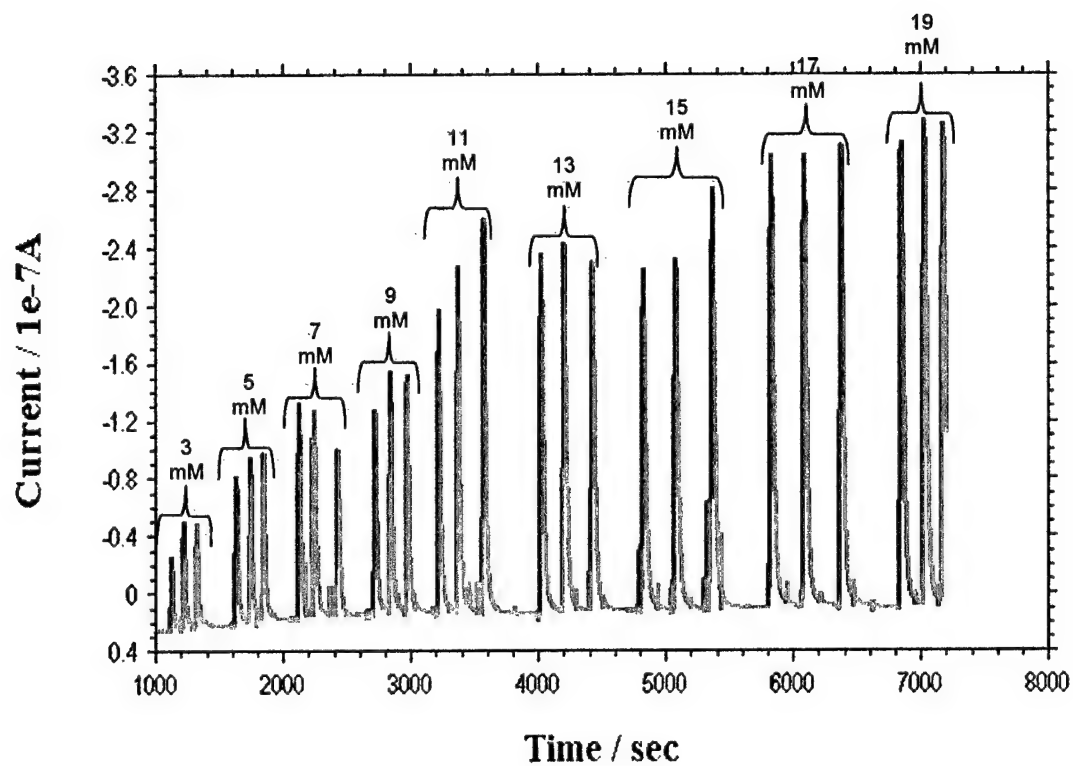


**Figure 34.** Flow injection analysis of glucose at the paste electrode containing 28 wt. % Azure A Eosinate under argon. Numbers indicate the concentrations of glucose solutions injected into the flow system. Potential, 0.0 V. Carrier solution, pH 7.40 phosphate buffer.

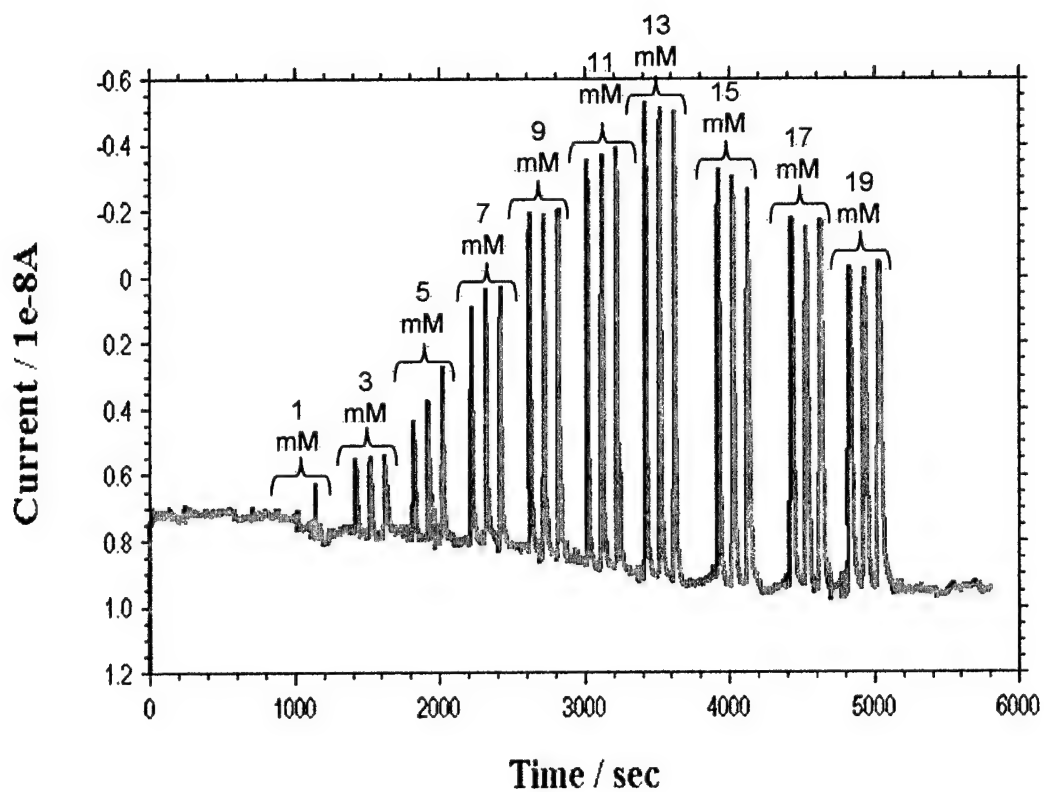


**Figure 35.** Flow injection analysis of glucose at the paste electrode containing 40 wt. % Azure A Eosinate under argon. Numbers indicate the concentrations of glucose solutions injected into the flow system. Potential, 0.0 V. Carrier solution, pH 7.40 phosphate buffer.

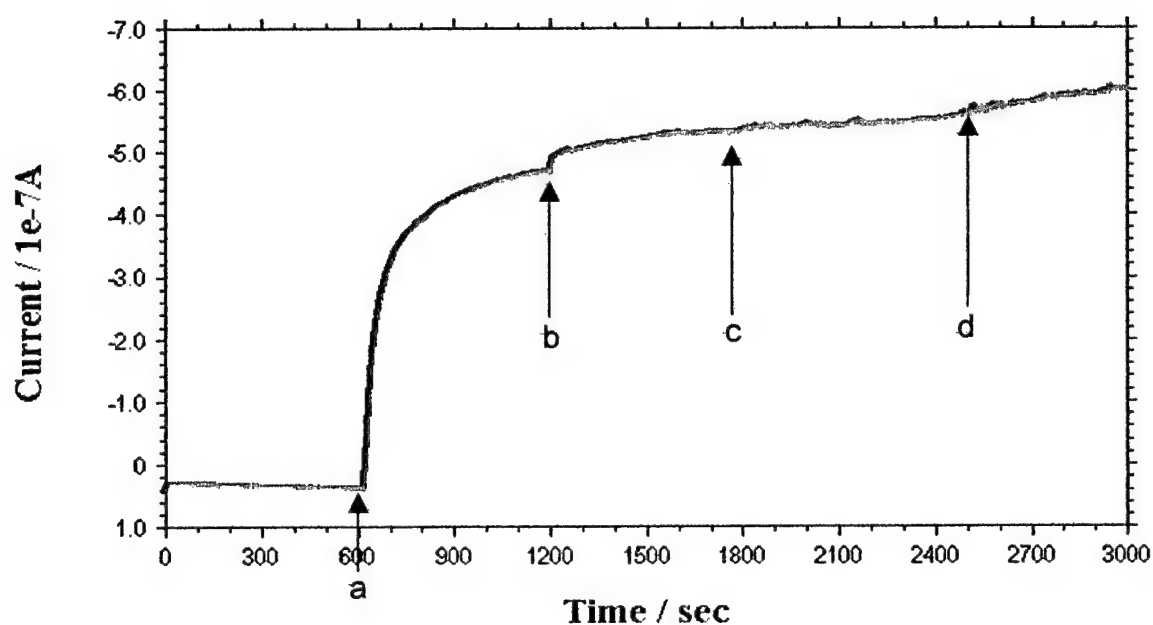


**Figure 36.** An amperometric trace recorded at the paste electrode (28 wt. % Azure A Eosinate) in a stirred solution that was spiked with (a) 5 mM glucose, (b) 0.10 mM ascorbic acid, (c) 0.10 mM acetaminophen, and (d) 0.10 mM uric acid. Background electrolyte, pH 7.40 phosphate buffer. Potential, 0.0 V.

at a low potential of 0.0 V, glucose detection is practically not disturbed by the presence of interfering species in the solution (the interference from ascorbic acid is < 7 %). The response of the paste electrode with 40 wt. % Azure A Eosinate was influence by the uric acid (Figure 37). The interference from uric acid is visible because the low sensitivity of this electrode required a sensitive current scale ( $10^{-8}$  A) to be used in order to see the glucose signal.

The operational stability of the paste electrodes was investigated in a flow system. Figure 38 shows that the electrode (28 wt. % Azure A Eosinate) response to 5 mM glucose was stable within  $\pm 5$  % for at least 12 hours under continuous polarization and continuous flow of the glucose carrier solution. This is an extraordinary biosensing performance, considering the simplicity of the biosensor preparation. A review of the literature indicates that such an operational stability is an exception rather than a rule in the case of electrochemical biosensors. For comparison purposes, Figure 39 shows a test of the operational stability of the paste electrode containing 40 wt. % Azure A Eosinate. Here, the signal decreased during the first 6 h to  $\sim 50$  % of the initial value, and thereafter stabilized during the remaining 7 hours.

### 3.2 CONCLUSIONS – PART 3

An efficient coupling of the glucose oxidase/glucose reaction to the electrode was accomplished by incorporating the enzyme and Azure A Eosinate mediator into the paste electrode. Such an electrode (biosensor) can operate at a very low sensing

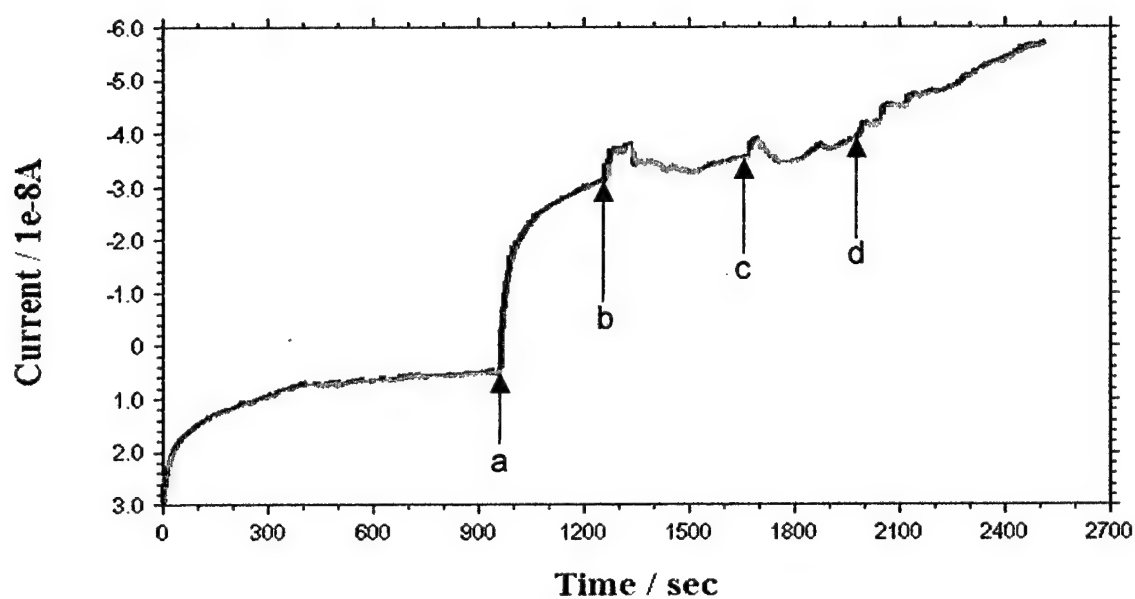


**Figure 37.** An amperometric trace recorded at the paste electrode (40 wt. % Azure B Eosinate) in a stirred solution that was spiked with (a) 5 mM glucose, (b) 0.10 mM ascorbic acid, (c) 0.10 mM acetaminophen, and (d) 0.10 mM uric acid. Background electrolyte, pH 7.40 phosphate buffer. Potential, 0.0 V.

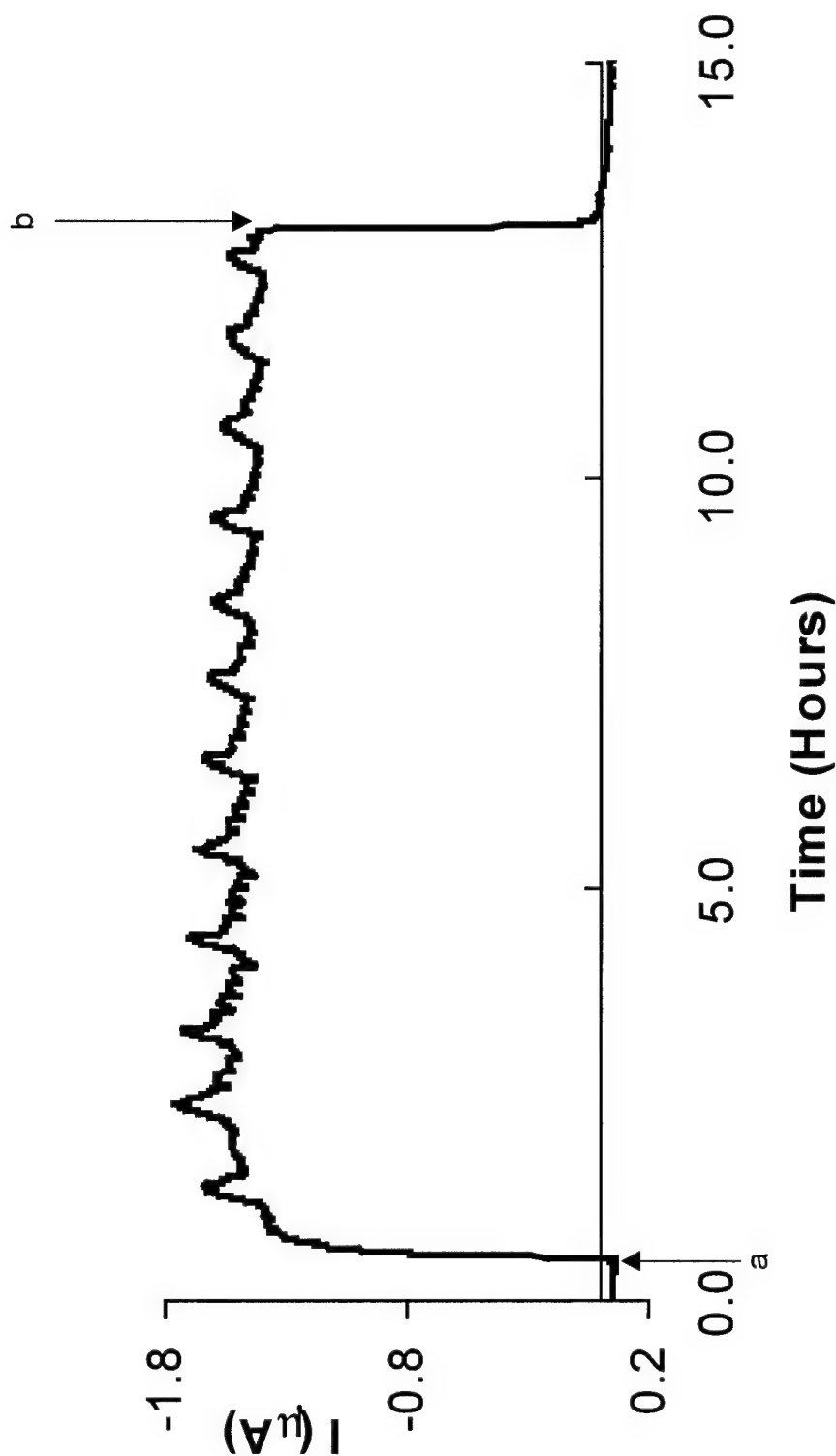


**Figure 38.** An amperometric trace recorded at the paste electrode (28 wt. % Azure A Eosinate) in a two-container flow system. Arrows indicate a moment of switching from the glucose-free carrier solution to the solution containing 5 mM glucose (a), and from 5 mM glucose solution back to the glucose-free solution. Background electrolyte, pH 7.40 phosphate buffer (0.05 M). Potential, 0.0 V. Flow rate, 0.1 mL min<sup>-1</sup>. The current spikes are artifacts caused by the flow system setup.

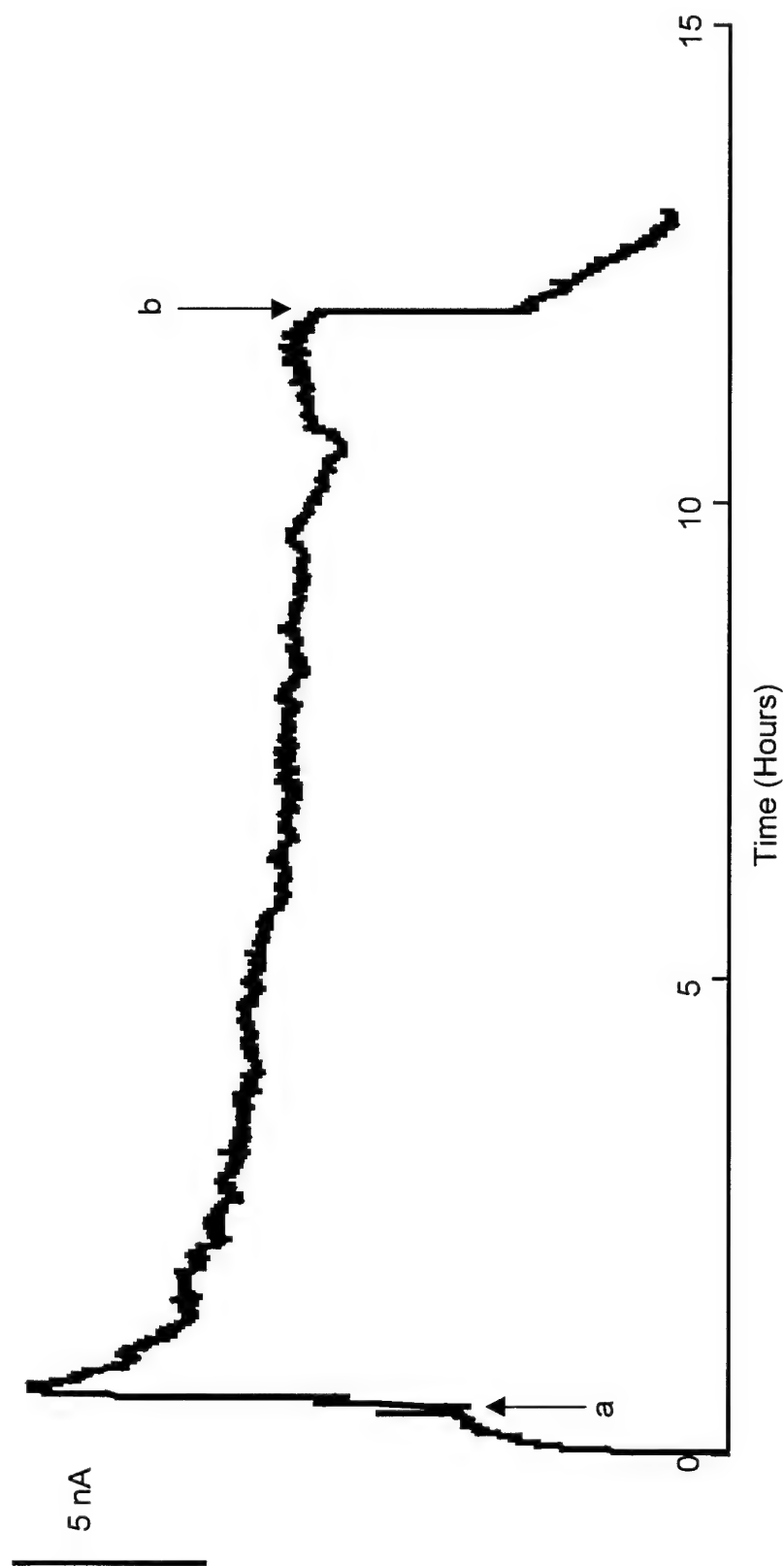


**Figure 39.** An amperometric trace recorded at the paste electrode (40 wt. % Azure A Eosinate) in a two-container flow system. Arrows indicate a moment of switching from the glucose-free carrier solution to the solution containing 5 mM glucose (a), and from 5 mM glucose solution back to glucose-free solution. Background electrolyte, pH 7.40 phosphate buffer (0.05 M). Potential, 0.0 V. Flow rate,  $0.1 \text{ mL min}^{-1}$ .

potential (0.0 V) due to the low standard potential of the azure redox couple. The low operating potential of the biosensor allows for an interference-free determination of glucose. The paste electrode displays an excellent operational stability in a flow system. The design of the paste electrode is very simple and generic, and can incorporate oxidoreductase enzymes other than glucose oxidase to provide a host of biosensors for biologically and environmentally important analytes.

## REFERENCES

- 1 Raba, J.; Mottola, H. *Crit. Rev. in Anal. Chem.* **1995**, 25, 1.
- 2 Onda, M.; Ariga, K.; Kunitake, T. *J. Biosci. Bioeng.* **1999**, 87, 69.
- 3 Turner, A. P. F.; Karube, I.; Wilson, G. S., (Eds.), *Biosensors Fundamentals and Applications*, Oxford University Press, Oxford, 1989, and references cited therein.
- 4 Cass, A. E. G., (Ed.), *Biosensors: A Practical Approach*, Oxford University Press, Oxford, 1990, and references cited therein.
- 5 Reach, G.; Wilson, G. S. *Anal. Chem.* **1992**, 64, 381A.
- 6 Miao, Y.; Tan, S. *Anal. Chim. Acta* **2001**, 437, 87.
- 7 Xiao, Y.; Ju, H.; Chen, H. *Anal. Chim. Acta* **1999**, 391, 299.
- 8 Brunetti, B.; Ugo, P.; Moretto, L.; Martin, C. *J. Electroanal. Chem.* **2000**, 491, 166.
- 9 Du, G.; Lin, C.; Bocarsly, A. B. *Anal. Chem.* **1996**, 68, 796.
- 10 Wilson, G.; Hu, Y. *Chem. Rev.* **2000**, 100, 2693.
- 11 Cass, A.; Davis, G.; Francis, G.; Hill, H.; Aston, W.; Higgins, I.; Plotkin, E.; Scott, L.; Turner, A. *Anal. Chem.* **1984**, 56, 667.
- 12 Liaudet, E.; Battaglini, F.; Calvo, E. *J. Electroanal. Chem.* **1990**, 293, 55.
- 13 Gregg, B.; Heller, A. *J. Phys. Chem.* **1991**, 95, 5970.
- 14 Ohara, T.; Rajagopalan, R.; Heller, A. *Anal. Chem.* **1994**, 66, 2451.
- 15 Zakeeruddin, S.; Fraser, D.; Nazeeruddin, M.; Gratzel, M. *J. Electroanal. Chem.* **1992**, 337, 253.
- 16 Crumbliss, A.; Hill, H.; Page, D. *J. Electroanal. Chem.* **1986**, 206, 327.
- 17 Morris, N.; Cardosi, M.; Birch, B.; Turner, A. *Electroanal.* **1992**, 4, 1.
- 18 Taniguchi, I.; Miyamoto, S.; Tomimura, S.; Hawkridge, F. *J. Electroanal. Chem.* **1988**, 240, 333.
- 19 Bartlet, P.; Ali, Z.; Eastwick-Field, V., *J. Chem. Soc. Farad. Trans.* **1992**, 88, 2677.
- 20 Hale, P.; Boguslavsky, L.; Karan, H.; Lan, H.; Lee, H.; Okamoto, Y.; Skotheim, T. *Anal. Chim. Acta* **1991**, 248, 155.

- 21 Kulys, J. J. *Biosensors* **1986**, 2, 3.
- 22 Turner, A.; Hendry, S.; Cardosi, M. *Biosensors: Instrumentation and Processing, The World Biotechnology Report, 1987*, Online Publications, London, **1987**, Vol. 1 (Part 3).
- 23 Martens, N.; Hindle, A.; Hall, E. *Biosens. Bioelectron.* **1995**, 10, 393.
- 24 Patolsky, F.; Tao, G.; Katz, E.; Willner, I. *J. Electroanal. Chem.* **1998**, 454, 9.
- 25 Krikstopaitis, K.; Kulys, J. *Electrochem. Commun.* **2000**, 2, 119.
- 26 Dicu, D.; Muresan, L.; Popescu, I.; Cristea, C.; Silberg, I.; Brouant, P. *Electrochim. Acta.* **2000**, 45, 3951.
- 27 Cenas, N. K.; Kulys, J. *Bioelectrochem. Bioenerg.* **1981**, 8, 103.
- 28 Narasimhan, K.; Wingard, L. B., Jr. *Anal. Chem.* **1986**, 58, 2984.
- 29 Centonze, D.; Losito, I.; Malitesta, C.; Palmisano, F.; Zambonin, P. G. *J. Electroanal. Chem.* **1997**, 435, 103.
- 30 Hecht, H. J.; Kalisz, H. M.; Hendle, J.; Schmid, R. D.; Schomburg, D. *J. Molec. Biol.* **1993**, 229, 153.
- 31 Jonsson, G.; Gorton, L. *Biosensors* **1985**, 1, 355-368
- 32 Cai, C.-X.; Xue, K.-H. *J. Electroanal. Chem.* **1997**, 427, 147.
- 33 Nakaminami, T.; Kuwabata, S.; Yoneyama, H. *Anal. Chem.* **1997**, 69, 2367.
- 34 Kirstein, D.; Kirstein, L.; Scheller, F.; Borcherdig, H.; Ronnenberg, J.; Diekmann, S.; Steinrucke, P. *J. Electroanal. Chem.* **1999**, 474, 43.
- 35 Bard, A. J.; Faulkner, L. R.; *Electrochemical Methods*, J. Wiley: New York, 1980.
- 36 Bianco, P.; Haladjian, J.; Bourdillon, C. J. *Electroanal. Chem.* **1990**, 293, 151.
- 37 Sasso, S. V.; Pierce, R. J.; Walla, R.; Yacynych, M. *Anal. Chem.* **1990**, 62, 1111.
- 38 Cass, A. E. G.; Davis, G.; Francis, G. D.; Hill, H. A. O.; Aston, W. J.; Higgins, J. I.; Plotkin, E. V.; Scott, L. D. L.; Turner, A. P. F. *Anal. Chem.* **1984**, 56, 667.
- 39 Kamin, R. A.; Wilson, G. S. *Anal. Chem.* **1980**, 52, 1198.
- 40 Pentano, P.; Kuhr, W. G. *Anal. Chem.* **1993**, 65, 623.
- 41 Bourdillon, C.; Demaille, C.; Gueris, j.; Moiroux, J.; Saveant, J.-M. *J. Am. Chem. Soc.* **1993**, 115, 12264.

- 42 Katz, E.; Heleg-Shabtai, V.; Bardea, A.; Willner, I.; Rau, H. K.; Haehnel, W. *Biosens. Bioelectron.* **1998**, *13*, 741.
- 43 Zhang, Y.; Hu, Y.; Wilson, G. S.; Moatti-Sirat, D.; Poitout, V.; Reach, G. *Anal. Chem.* **1994**, *66*, 1183-1188.
- 44 Bartlett, P. N.; Cooper, J. M. *J. Electroanal. Chem.* **1993**, *362*, 1.
- 45 Yon Hin, B. F. Y.; Smolander, M.; Crompton, T.; Lowe, C. R. *Anal. Chem.* **1993**, *65*, 2067.
- 46 Palmisano, F.; Zambonin, P. G.; Centonze, D. *Fresenius J. Anal. Chem.* **2000**, *366*, 586.
- 47 Ohara, T. J.; Rajagopalan, R.; Heller, A. *Anal. Chem.* **1994**, *66*, 2451.
- 48 Binyamin, G.; Cole, J.; Heller, A. *J. Electrochem. Soc.* **2000**, *147*, 2780.
- 49 Bu, H. Z.; English, A. M.; Mikkelsen, S. R. *Anal. Chem.* **1996**, *68*, 3951.
- 50 Dave, B. C.; Dunn, B.; Valentine, J. S.; Zink, J. I. *Anal. Chem.* **1994**, *66*, 1120A.
- 51 Sampath, S.; Lev, O. J. *Electroanal. Chem.* **1997**, *426*, 131.
- 52 Matuszewski, W.; Trojanowicz, M. *Analyst (London)* **1988**, *113*, 735.
- 53 Wang, J.; Lu, F. *J. Am. Chem. Soc.* **1998**, *120*, 1048.
- 54 Schumacher, J. T.; Munch, I.; Richter, T.; Rohm, I.; Bilitewski, U. *J. Mol. Catal.* **1999**, *7*, 67.
- 55 Wang, J.; Varughese, K. *Anal. Chem.* **1990**, *62*, 318.
- 56 Cespedes, F.; Alegret, S. *Trends Anal. Chem.* **2000**, *19*, 276.
- 57 Moore, G.; Roberts, G. *Internat. J. Biol. Macromol.* **1981**, *3*, 73.
- 58 Muzzarelli, R. A. A. *Chitin*; Pergamon Press: Oxford, 1977.
- 59 Krajewska, B. *Acta Biotechnol.* **1991**, *11*, 269.
- 60 Spagna, G.; Andreani, F.; Seletelli, E.; Romagnoli, D.; Pifferi, P. G. *Process Biochem.* **1998**, *33*, 57.
- 61 Hikima, S.; Kakizaki, T.; Taga, M.; Hasebe, K. *Fresenius J. Anal. Chem.* **1993**, *345*, 607.
- 62 Ng, L.-T.; Yuan, Y. J.; Zhao, H. *Electroanalysis* **1998**, *10*, 1119.
- 63 Wang, G.; Xu, J.-J.; Ye, L.-H.; Zhu, J.-J.; Chen, H.-Y. *Bioelectrochemistry* **2001**, *5650*,

- 64 Okuma, H.; Watanabe, E. *Biosens. Bioelectron.* **2002**, 17, 367.
- 65 Adams, R. N. *Anal. Chem.* **1958**, 30, 1576.
- 66 Svancara, I.; Vytras, K.; Barek, J.; Zima, J. *Crit. Rev. in Anal. Chem.* **2001**, 31, 311 (and references therein).
- 67 Kulys, J.; Hansen, H.; Buch-Rasmussen, T.; Wang, J.; Ozsoz, M. *Anal. Chim. Acta* **1994**, 288, 193.
- 68 Bauer, D.; Gaillochet, M. P. *Electrochim. Acta* **1974**, 19, 597.
- 69 Ravinchandran, K.; Baldwin, R. P. *J. Electroanal. Chem.* **1981**, 126, 293.
- 70 Matuszewski, W.; Trojanowicz, M. *Analyst* **1988**, 113, 735.

## VITA

Lucy Lim was born in Milwaukee, Wisconsin [REDACTED] the daughter of Frank and Antonina Porada. She received her Bachelor of Science with a major in Biology from Marquette University in August 1981. She received a Master of Science with a major in Microbiology from Abilene Christian University in December 1988. She taught Microbiology at the Abilene Christian and McMurry Universities in Abilene, TX. She worked at Fairleigh Dickinson Research Laboratory and hospital laboratories in Abilene and San Antonio, TX. She entered the United States Air Force as a Captain in January 1995. In August 2000, she entered the Graduate School of The University of Texas at San Antonio via the Air Force Institute of Technology (AFIT) program. She was directly promoted to the rank of Major in August 2001.